International Journal of Plasticity, 149 (2022) 103183 https://doi.org/10.1016/j.ijplas.2021.103183

Size-dependent yield stress in ultrafine-grained polycrystals: A multiscale discrete dislocation dynamics study

Songjiang Lu[a], Qianhua Kan[a], Michael Zaiser[b], Zhenhuan Li[c], Guozheng Kang[a], Xu Zhang[a*]

[a]*Applied Mechanics and Structure Safety Key Laboratory of Sichuan Province, School of Mechanics and Engineering, Southwest Jiaotong University, Chengdu 610031, China*

[b]*Department of Materials Science and Engineering, Institute of Materials Simulation WW8, FAU University of Erlangen-Nuremberg, Dr.-Mack-Str.77, 90762 Fürth, Germany*

[c]*Department of Mechanics, School of Aerospace Engineering, Huazhong University of Science and Technology, Wuhan, 430074, China*

**Correspondent authors E-mails: xzhang@swjtu.edu.cn (XZ)*

Homepage: https://faculty.swjtu.edu.cn/xu_zhang/

Graphical abstract

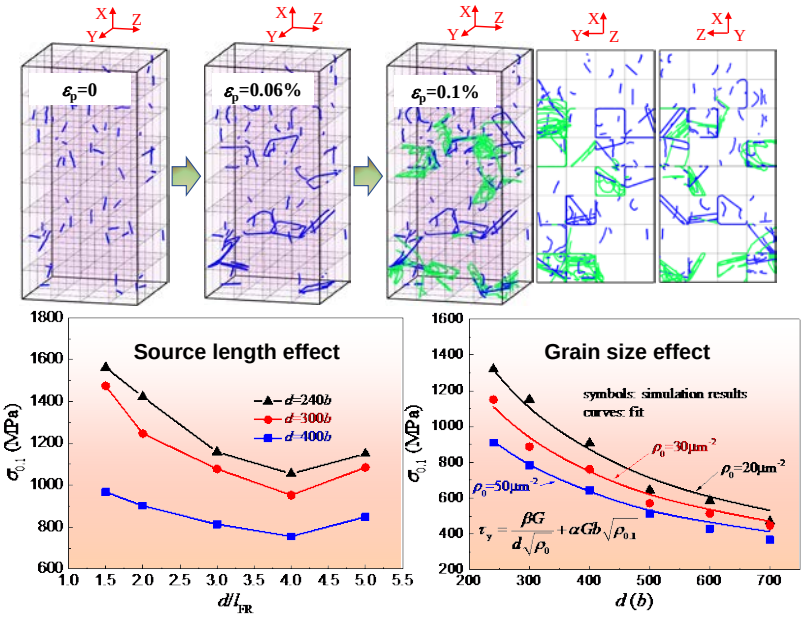

Highlights

- A polycrystal model containing > 100 grains with dislocation-penetrable grain boundaries was constructed within a discrete dislocation dynamics framework.
- The effects of dislocation source parameters and grain size on the yield stress of ultrafine-grained polycrystals were systematically studied.
- In the initial, grain boundary dominated regime, the change of dislocation density is proportional to plastic strain and independent of the initial dislocation density.
- The combined effects of source length, grain size, and initial dislocation density on flow stress can be captured by a single equation.

Abstract

In this study, the effects of grain size and dislocation source properties on the yield stress of ultrafine-grained (UFG) polycrystals were examined using three-dimensional multiscale discrete dislocation dynamics (DDD). A polycrystal model containing multiple grains with randomly distributed orientations was constructed within a multiscale DDD framework. Grain boundaries (GBs) were assumed to be penetrable by dislocations, with two dislocation-GB interaction mechanisms, i.e., dislocation absorption at GBs and dislocation emission from GBs, being considered. The simulation investigated the dislocation source effect and demonstrated a non-monotonic dependency of flow stress on dislocation source length, where the lowest flow stress corresponds to a Frank-Read (FR) source length of $d/4$ where d is the grain size. When the length of a FR source in the polycrystalline sample exceeds this value, the simulated yield stress increases owing to the constraining effect of grain boundaries on dislocation movement. The grain size dependence of the yield stress shows deviations from the classical Hall–Petch relationship as the exponent in the Hall–Petch type relation ranges from about 0.91 to about 0.98, depending on the initial dislocation density in the samples. Detailed analysis indicates that the grain size dependence of the yield stress is mainly controlled by the effect of grain boundary constraints on dislocation activation. A secondary effect arises from grain size dependent dislocation accumulation and the resulting Taylor hardening. The activation and operation of FR sources were quantitatively examined to further understand the origins of source length and grain size effects. A theoretical model is proposed to account simultaneously for the effects of source length, grain size, and initial dislocation density on the yield stress of polycrystals in the UFG regime.

Keywords: Dislocation dynamics; Polycrystals; Grain boundary; Grain-size dependence; Dislocation source effect

1. Introduction

Mechanical properties of polycrystalline metals are closely related to parameters of their microstructure, such as grain size and initial dislocation arrangement. It has been widely observed in experiments that the yield stress of polycrystalline metals increases with decreasing grain size, as described by the well-known "Hall–Petch law" (Hall, 1951; Petch, 1953):

$$\sigma_{\mathrm{y}} = \sigma_0 + k_{\mathrm{HP}} d^{-1/2} \tag{1}$$

where σ_{y} denotes the yield stress and d denotes the grain size of polycrystalline metals. k_{HP} is a material property and usually called the Hall–Petch (HP) constant, σ_0 ideally is the yield stress of a single crystal or can be regarded as the yield stress of a very coarse-grained, untextured polycrystal. The HP relation has been widely used to describe the grain size dependence of yield stress for a variety of metals. However, whether or not the yield stress of polycrystalline metals scales with the inverse square root of grain size, $d^{-1/2}$, as well as the physical origins of such a relationship, is still a matter of debate (Cordero et al., 2016; Jiang et al., 2021; Lefebvre et al., 2007). For example, many experimental studies show that the exponent of grain size d in Eq. (1) roughly ranges from –0.5 to –1 (Keller et al., 1998; Ohno and Okumura, 2007; Venkatraman and Bravman, 1992; Yu and Spaepen, 2004). In a number of numerical investigations (Balint et al., 2008; Borg, 2007; Evers et al., 2004), this exponent was even found to be smaller than –1, depending on initial dislocation density, grain size range, and plastic strain offset used in the definition of yield stress. Moreover, (Dunstan and Bushby, 2013, 2014) summarized and analyzed experimental data published in the literature for various metals and concluded that the grain size dependence of yield stress was better described by proportionality to $1/d$ or $\ln(d)/d$. In order to understand these differences in the form of the grain size dependence in polycrystalline metals, further study considering microstructure evolution is required to reveal the mechanisms underlying the grain size effect.

In the last three decades, discrete dislocation dynamics (DDD) has been established as an efficient tool for studying the physical mechanisms governing

deformation of crystalline materials at the micro- and nanoscale (Bertin et al., 2020; Chatterjee et al., 2021; Cui et al., 2014; Fan et al., 2018; Guo et al., 2021; Huang et al., 2020; Xu et al., 2021; Záležák et al., 2017). By the DDD approach, the temporal evolution of interacting dislocations, the ensuing dynamics of plastic flow, and the evolution of dislocation microstructures during deformation can be efficiently captured. There are many studies using two-dimensional (2D) DDD to investigate the plasticity of polycrystalline metals (Balint et al., 2008; Biner and Morris, 2002, 2003; Huang et al., 2020; Lefebvre et al., 2007; Leung and Ngan, 2013; Li et al., 2009; Quek et al., 2016). (Balint et al., 2008) conducted 2D DDD simulations with an impenetrable GB model to probe the effect of dislocation slip incompatibility and initial dislocation source density on the grain size dependence of yield stress. (Li et al., 2009) performed 2D DDD simulations with an impenetrable or penetrable GB model to study the grain size effect of polycrystals, predicting the exponent of grain size d in Eq. (1) to range from 0.62 to 0.85, 0.73 to 0.95 and 0.71 to 1.05, depending on the definition of the yield stress. (Lefebvre et al., 2007) investigated the dislocation mechanisms dominating the effect of grain size on the tensile plastic deformation of ultrafine-grained polycrystalline metals under multiple slip conditions using 2D DDD simulation. Furthermore, 2D DDD has also been widely used to investigate the grain size and thickness effects of polycrystalline thin films (Kumar et al., 2010; Nicola et al., 2005; Nicola et al., 2006; Shishvan and Van der Giessen, 2010; von Blanckenhagen et al., 2004; von Blanckenhagen et al., 2003), the sample size effect in the compression of micro-pillars (e.g. (Guruprasad and Benzerga, 2008)), the indentation size effect (e.g. (Balint et al., 2006; Xu et al., 2019)) and the contact size effect in thin films (e.g. (Xu et al., 2021)).

The 2D DDD models have provided useful insights into the plastic deformation of polycrystalline metals at the submicron scale. However, compared with three-dimensional (3D) DDD frameworks, the 2D models cannot effectively capture complex dislocation reactions (such as cross slip and junction formation) and long-range dislocation stress-field effects and thus may not provide a full description of polycrystal deformation. Most importantly, in any 2D model the action of

dislocation sources needs to be represented by *ad hoc* rules; hence, such models are by construction unsuitable for studying effects of source length and source configuration. There are a few studies using 3D DDD to investigate the plastic deformation of polycrystals (De Sansal et al., 2010; Espinosa et al., 2005; Espinosa et al., 2006; Jiang et al., 2019; Yellakara and Wang, 2014; Zhou and LeSar, 2012). Espinosa et al. (Espinosa et al., 2005; Espinosa et al., 2006) carried out 3D DDD simulations on polycrystalline thin films to investigate the film thickness and grain size effects based on the assumption that dislocations are mainly nucleated at grain boundaries. (Yellakara and Wang, 2014) investigated the effects of grain size, grain shape, and initial dislocation density on the yield stress and the HP relationship of polycrystalline copper. The studies mentioned above used only one grain (simulation cell) to represent the polycrystalline metals in the DDD framework, and the GBs were assumed to impenetrable to dislocation transmission, which might not fully capture the real physical features of dislocation-GB interactions. (De Sansal et al., 2010) constructed a polycrystal model containing 16 regular polyhedral grains with randomly selected orientations to investigate the plasticity of microcrystalline copper. They reported the HP exponent of the yield stress in their simulations to vary between −1/2 and −1. However, also here the GBs were considered as impenetrable dislocation obstacles. Considering the limitations of previously proposed DDD models in simulating the deformation of polycrystalline metals, it is worthwhile to construct a more realistic polycrystal model containing multiple, randomly oriented grains and penetrable GBs in a 3D DDD framework.

In addition to the effect of grain size in polycrystalline metals, the length of pre-existing Frank-Read (FR) sources in the samples may also play a crucial role in controlling the yield stress. Von Blanckenhagen et al. (von Blanckenhagen et al., 2004; von Blanckenhagen et al., 2001a, b, 2003) conducted a series of simulations using 3D DDD and found that the lowest yield stress was associated with a FR source length around $d/4$ and $d/3$ for the cases with and without dislocation pile-ups in front of GBs, respectively. (Ohashi et al., 2007) performed a similar DDD simulation and obtained an identical conclusion, namely that the critical stress to generate a full dislocation

loop in a grain was lowest when the length of the FR source was $l_{FR}=d/3$. In these studies, the polycrystalline aggregate was simplified as one cube-shaped single grain with surfaces treated as impenetrable barriers to dislocation motion. Besides, there was only one dislocation source with a fixed length positioned in the center of the grain. This over-simplified model does not fully capture the nature of dislocation interactions with and across GBs in a polycrystalline aggregate and is therefore unlikely to provide an accurate description of yielding as a process involving many grains.

In the current study, we construct a DDD polycrystal model containing multiple grains with randomly distributed orientations. The GB model embedded within this DDD framework considers two dislocation-GB interaction mechanisms, i.e., dislocation absorption at GBs and dislocation emission from GBs. This GB model uses a 'coarse-graining' approach to handle the complex process of dislocation-GB interactions for arbitrary GB types without much loss of physics. Details of this model were described in (Zhang et al., 2021). In the present investigation, we use this DDD framework to investigate the effect of FR source length, grain size and initial dislocation density on the yield stress of ultrafine-grained polycrystalline metals. To the best knowledge of the authors, this is the first work to simulate the behavior of polycrystals by applying the 3D DDD method to a sufficiently large grain assembly (> 100 grains) with dislocation-penetrable GBs.

2. Simulation method

2.1 Multiscale DDD framework

In the present study, a hybrid model (multiscale DDD model) (Huang et al., 2017; Lu et al., 2019; Zbib and Diaz de la Rubia, 2002; Zbib et al., 1998) coupling discrete dislocation dynamics (DDD) with the finite element method (FEM) is used to perform simulations on polycrystalline metals. This type of multiscale framework was originally developed by (Zbib and Diaz de la Rubia, 2002; Zbib et al., 1998) and recently improved by (Huang et al., 2017) and (Vattré et al., 2014). In this method, a segment-based discrete description of the interaction of close dislocations is coupled

to a coarse-grained description of the plastic eigenstrain, which is transferred from DDD to FEM to evaluate an elastic-plastic boundary value problem, with the ensuing stress field transferred back from FEM to DDD. Segment-based stress corrections are defined to match the FEM stress field to address the underestimated interaction between close dislocations faced in earlier DDD-FEM coupling frameworks. Further details of this hybrid scheme can be found in (Huang and Li, 2015; Huang et al., 2017; Jamond et al., 2016; Vattré et al., 2014).

2.2 Polycrystal model

The polycrystal model used in the present work extends the model of a bicrystal with a penetrable GB formulated in (Zhang et al., 2021) to a face-centered cubic (fcc) polycrystal sample. The simulated sample consists of 4×4×8 cube-shaped grains with equal edge length d forming a regular grid-like stacking as shown in Fig. 1a. Orientations of the fcc crystal lattice were assigned randomly to the cubic crystallites. We note that (Huang et al., 2020), who consider a similar morphology consisting of cube shaped grains, report that a more realistic Voronoi construction yields similar results for the same average grain size. The sample is loaded in the direction of its long axis (X-axis in Fig. 1a) by fully constraining the bottom of the model (plane $x=-4d$) and imposing a uniaxial displacement in $-X$ direction on the top surface (plane $x=4d$). The imposed displacement rate of $40000d\ s^{-1}$ induces a constant average strain rate of $5000\ s^{-1}$. Since we used 3D DDD to simulate a polycrystalline sample with multiple grains, the computational load is significant especially for the larger samples. Therefore, a relatively high loading rate was chosen to enhance computational efficiency (see for comparison (Bayerschen et al., 2015; Fan et al., 2016; Guo et al., 2021; Srivastava and El-Awady, 2017). We note that according to criteria given by (Fan et al., 2021), the present simulations are well inside the regime of low rate sensitivity; hence, even a significant reduction of strain rate is not expected to change the results. This is also borne out by our own sensitivity checks which indicate that a reduction in strain rate by a factor 10 reduces the flow stresses in our simulations by less than 15%. This finding is in line with experimental observations of a moderate

strain-rate sensitivity of UFG Cu and Ni samples by (Gray et al., 1997) who report moderate variations in yield stress by 15-25% over the strain rate range from 10^{-3} s^{-1} to 3000 s^{-1}. We therefore do not explicitly consider strain rate effects in the remainder of this study.

The side surfaces of the sample are treated as free surfaces in the elastic boundary value problem; on these surfaces, dislocations are allowed to freely escape according to the local stress state. In the present study, an assembly of Frank-Read (FR) type sources is chosen as initial dislocation configuration in order to mimic the fragmented network present in UFG materials. This allows us to control the initial dislocation density and source length in terms of the spacing and number of pinning points. In particular, the presence of sources with strong pinning points avoids the problem of dislocation starvation which may, in UFG structures, occur with other initial conditions (e.g. straight grain-threading dislocations) already at small strains. For these reasons, this type of initial configuration has been widely adopted in DDD studies of the plasticity of polycrystalline metals with the grain size at the nano- or micro-scale (Ohashi et al., 2007; von Blanckenhagen et al., 2004; von Blanckenhagen et al., 2001a, b, 2003; Yellakara and Wang, 2014; Zhou and LeSar, 2012). For each sample, initial FR dislocation sources are randomly distributed in the whole simulated volume under the constraint that the dislocation lines are not allowed to intersect any GB planes, as shown in Fig. 1b. The material simulated in this paper is taken to be face-centered cubic (fcc) aluminum with shear modulus G=26 GPa and Poisson ratio v=0.345. The magnitude b of the Burgers vector is taken as 0.25 nm, and the viscous drag coefficient of dislocation motion is 10^{-4} Pa·s. The GB parameters used here are the same as those in our former work describing the GB model (Zhang et al., 2021). Note that there is only one set of slip systems for fcc crystals, i.e. {111}<110>, which includes 12 different slip systems. In our simulations, all 12 slip systems are considered in each grain, initial FR dislocation sources are randomly distributed on these slip systems.

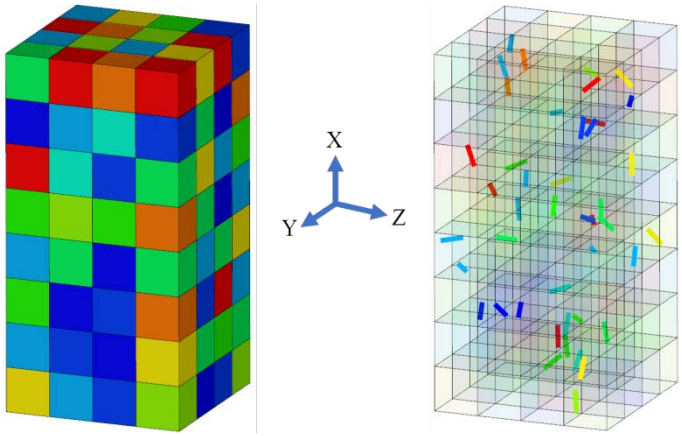

(a) (b)

Fig. 1. Geometry model. (a) Polycrystal model containing multiple cube-shaped grains with randomly distributed orientations, (b) example of FR dislocation source distribution in the model.

2.3 GB model

In the present work, we adopt a 3D penetrable GB model proposed in (Zhang et al., 2021) to handle the interactions between dislocations and GBs in polycrystals. In this model, two GB-dislocation interaction scenarios were considered, namely, dislocation absorption at GBs and dislocation emission from GBs. Since the dislocation lines piled up at GBs are irregular for non-symmetrical GB types, it is difficult to represent all details of dislocation transmission of dislocations across the GB plane accurately within the DDD framework. Hence, a coarse-graining approach is used to describe the main features of dislocation absorption and emission at GBs. In this approach, the GB plane is divided into elements with equal size. These elements are envisaged as dislocation sinks and/or dislocation sources for dislocation absorption at GBs and dislocation emission from GBs, respectively. Dislocation absorption is controlled by a critical stress condition, i.e. the resolved shear stress acting on the incoming dislocations must be larger than the GB strength τ_{gb} (Zhang et al., 2021). Dislocation emission events typically occur with assistance of the stress fields of dislocations that are piled up on the other side of the grain boundary. The emission criterion is based on rules that include information specific to the emitted

dislocations such as grain association, slip plane, Burgers vector, etc. as well as parameters describing the internal state of the grain boundary (Zhang et al., 2021).

One modification of the bicrystal model (Zhang et al., 2021) concerns the GB strength τ_{gb}, which is correlated with the GB energy E_{gb} by $\tau_{gb}=E_{gb}/b$. The parameter τ_{gb} is important since it controls dislocation absorption at GBs and thereby influences the behavior of plastic deformation. In our previous work investigating the mechanical behavior of bicrystalline pillars, the GB energy was evaluated from molecular dynamics simulation (Zhang et al., 2021). However, owing to a large number of GBs with different misorientations in the polycrystal model studied here, it is impractical to use molecular dynamics simulation to calculate the GB energies for all GBs due to the heavy computational burden. Instead, GB energies are computed using an interpolation scheme proposed by (Bulatov et al., 2014), who calculated GB energies for a large number of GB types and different materials. By defining a metric in the 3 x 2 dimensional space of possible GB configurations, they then developed a scheme where the energy of a generic GB is estimated by evaluating its metric distance from all GBs in the database and, after using these distances to evaluate strongly nonlinear weight functions, taking the weighted average of the respective GB energies. For details the reader is referred to (Bulatov et al., 2014), who also provide the GB data underlying their interpolation and the source code of the interpolation script under public license.

Note that by implementing the energy function proposed by Bulatov et al. into the DDD framework, the computation efficiency can greatly improve compared with that of using molecular dynamics simulations to calculate GB energies in the previous article (Zhang et al., 2021). This is mandatory in view of the large number of GBs in our samples and the fact that multiple statistical realizations of the polycrystalline aggregate must be simulated for each parameter set to obtain statistically reliable results.

3. Dislocation motion in polycrystals

3.1 Effect of source length and grain size on dislocation motion

The operation of a FR source in the interior of a grain of size d depends not only on the initial source length l_{FR} but also on the constraint imposed by the grain boundaries. To study the effect of the ratio d/l_{FR} on the yield stress of the samples, several model polycrystals with constant source lengths of $l_{FR}=d/1.5$, $l_{FR}=d/2$, $l_{FR}=d/3$, $l_{FR}=d/4$, $l_{FR}=d/5$ were simulated for three different grain sizes, $d=240b$, $d=300b$ and $d=400b$. In all simulations, the total number of grains was kept at 128, and the sample size changed in proportion with the grain size d. The initial dislocation density in all simulated cases was fixed at 20 μm^{-2}. It should be mentioned that five realizations with random distributions of grain orientations and FR sources were simulated for all sets of parameters. All results are averages over these realizations.

Fig. 2a plots the variation of 0.1% offset yield stress, $\sigma_{0.1}$ (the flow stress at a plastic strain of 0.1%), as a function of the ratio between the grain size and FR source length, d/l_{FR}, for three prescribed grain sizes. It shows that the yield stress increases with decreasing grain size, irrespective of d/l_{FR}, demonstrating a typical grain size effect. A detailed analysis of this effect will be presented in Section 4. From Fig. 2a, another interesting observation is that the lowest yield stress for all grain sizes is obtained at $d/l_{FR}=4$. In other words, when the FR source length is a quarter of the grain size, the polycrystalline sample has the lowest yield stress. We first compare this observation with the theoretical prediction for the case where the yield stress is controlled by activation of unconstrained bulk FR sources. The shear stress to activate such a source can be calculated through the following equation (Hirth and Lothe, 1982; Zhang et al., 2014):

$$\tau_{FR} = \frac{k}{2\pi}\frac{Gb}{l_{FR}}\log\frac{l_{FR}}{r} \tag{2}$$

where $k=1$ for edge and $k=1/(1-\nu)$ for screw dislocations. Since there are different types of dislocations (including edge, screw, and mixed ones) in the simulations, the parameter k is approximated as $k=[1+1/(1-\nu)]/2$ for simplicity. The parameter r is the Brown splitting distance and set as $2b$ (Zhang et al., 2014). The corresponding theoretical yield stress σ_{FR} is given by

$$\sigma_{\mathrm{FR}} = M\tau_{\mathrm{FR}} = \frac{Mk}{2\pi}\frac{Gb}{l_{\mathrm{FR}}}\log\frac{l_{\mathrm{FR}}}{r} \tag{3}$$

where the orientation factor M is here, in line with the Taylor model of a random polycrystal, chosen as M=3. According to Eq. (3), the yield stress will monotonically increase as d/l_{FR} increases for a specified grain size d, which is inconsistent with the simulation results shown in Fig. 2a. Fig. 2b presents the ratio between the simulated and theoretical yield stresses $\sigma_{0.1}/\sigma_{\mathrm{FR}}$ versus d/l_{FR}. It shows that the ratio $\sigma_{0.1}/\sigma_{\mathrm{FR}}$ increases as d/l_{FR} decreases when d/l_{FR} is smaller than 4, whereas the ratio keeps at a constant value of around 1 when d/l_{FR} is larger than 4. In other words, the yield stress of the polycrystalline sample approximately equals the value predicted from Eq. (3) when d/l_{FR} is greater than 4. The variation of $\sigma_{0.1}/\sigma_{\mathrm{FR}}$ with d/l_{FR} is mainly related to the constraint imposed by the GBs on the operation of FR sources.

Note that the yield stress is often taken as 0.2% proof stress in experiments and engineering. To verify whether our results are affected by the yield stress definition, we performed an additional simulation with plastic strain up to 0.2% for the case of d=300b. The 0.2% proof stress $\sigma_{0.2}$ versus d/l_{FR} for this case is plotted in Fig. 2a. It can be seen that because of the higher yield strain, the curve of $\sigma_{0.2}$ vs d/l_{FR} shows an approximately d independent offset which is due to the dislocation density increase and concomitant strain hardening from 0.1% to 0.2% plastic strain. The same behavior is seen in Fig. 2b which shows that both ratios $\sigma_{0.1}/\sigma_{\mathrm{FR}}$ and $\sigma_{0.2}/\sigma_{\mathrm{FR}}$ are independent of d/l_{FR} for $d/l_{\mathrm{FR}}\geq$4. Thus, our conclusions regarding the dependency of yield stress on grain size and source length are unaffected by the yield stress definition. For reasons of computational cost (Jiang et al., 2019) we have therefore, unless otherwise mentioned, used a 0.1% offset. A similar approach has also been adopted by other researchers (Balint et al., 2008; De Sansal et al., 2010; Jiang et al., 2019; Lefebvre et al., 2007).

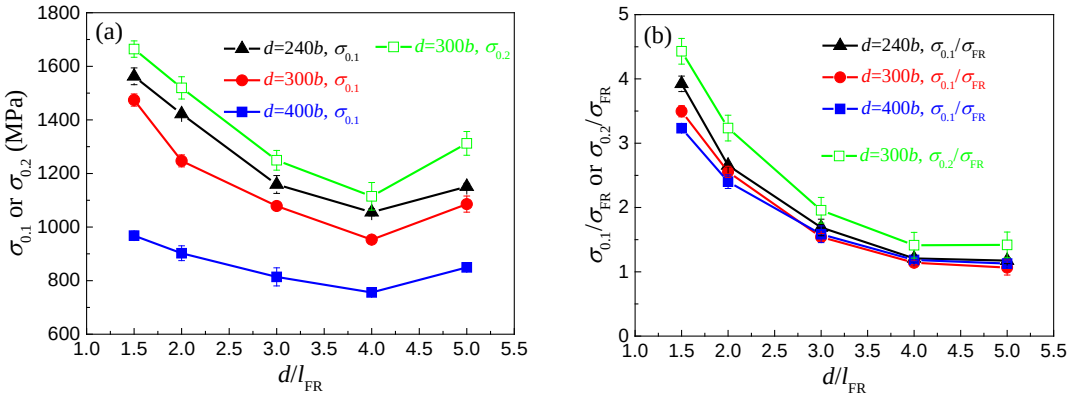

Fig. 2. Simulation results. (a) 0.1% or 0.2% offset yield stress $\sigma_{0.1}$ or $\sigma_{0.2}$ vs. the ratio d/l_{FR} of grain size to FR source length, for three different grain sizes, (b) the ratio $\sigma_{0.1}/\sigma_{FR}$ or $\sigma_{0.2}/\sigma_{FR}$ of the yield stress from simulation to the FR source strength predicted from Eq. (3), plotted vs. d/l_{FR} for three different grain sizes. The results are averaged over five realizations and the error bars represent the standard deviation.

Fig. 3 schematically illustrates the operation of a FR source in the grain center. As shown in Fig. 3, the initially straight FR source line with length l_{FR} gradually bows out under increasing shear stress. The expanding loop is then constrained by the GB. If the distance s between the GB and the pinning point of the FR source is smaller than l_{FR}, the stress required to move the dislocation further is controlled by s, whereas for s longer than l_{FR}, it is controlled by l_{FR}. For a model containing only one grain, the yield stress is usually defined as the critical stress required to emit only one dislocation loop from a FR source, as studied in (Ohashi et al., 2007; von Blanckenhagen et al., 2004; von Blanckenhagen et al., 2003). In such a case, the sample has the lowest yield stress when $d/l_{FR}=3$. However, in real polycrystalline metals, the sample starts to yield only when sufficient dislocation movements occur in the grain interior. Thus, the FR sources need to operate several times to reach the yield condition (both for the cases of GB with finite GB strength and impenetrable GB). As a result, dislocation pile-ups are generated in front of the GBs, leading to an effective shortening of s, as schematically shown in Fig. 3c. In this case, the d/l_{FR} value for the lowest yield stress is slightly larger than 3. A value of about 4 is obtained in our simulations, as shown in Fig. 2b.

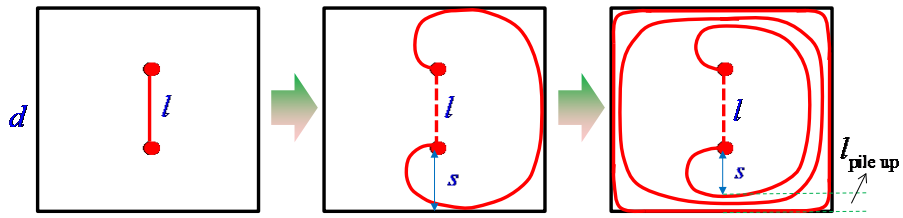

(a) (b) (c)

Fig. 3. Schematic illustration for the operation of a FR source.

It should be mentioned that the optimal source length of $l_{FR}=d/4$ inferred from Fig. 3 is based on the assumption that the FR source is initially positioned at the center of the grain and the slip plane of the dislocation has a square shape with a size of d. However, in the model polycrystals simulated here, the position and orientation of the FR sources, as well as the location of the corresponding slip plane, are randomly assigned, which seems to differ significantly from the situation illustrated in Fig. 3. (Ohashi et al., 2007) and (von Blanckenhagen et al., 2003) demonstrated that the activation stress would be higher when a FR source is located further away from the grain center. This suggests that the yield stress of the sample is controlled by the FR sources with a length of $l_{FR}=d/4$ residing near the center of the grain. From a statistical point of view, the model with randomly distributed sources must contain a certain number of sources located near the grain center, and these most effective (because they are weakest) sources dominate the yielding of the sample. Therefore, the schematic diagram shown in Fig. 3 to motivate the most effective source length as $l_{FR}=d/4$ in our simulations provides a reasonable picture of the actual situation.

The phenomenon of dislocation confinement schematically shown in Fig. 3 can also be observed during the dislocation evolution in the simulations. Fig. 4 shows the dislocation confinement by GBs for a sample with $d=300b$ and $d/l_{FR}=2$. It can be seen from Fig. 4 that a dislocation source stops continuously operating after the emitted segment reaches the GB surface since the distance between the corresponding pinning point and the GB is smaller than the initial FR length and thus the dislocation requires higher shear stress to move forward.

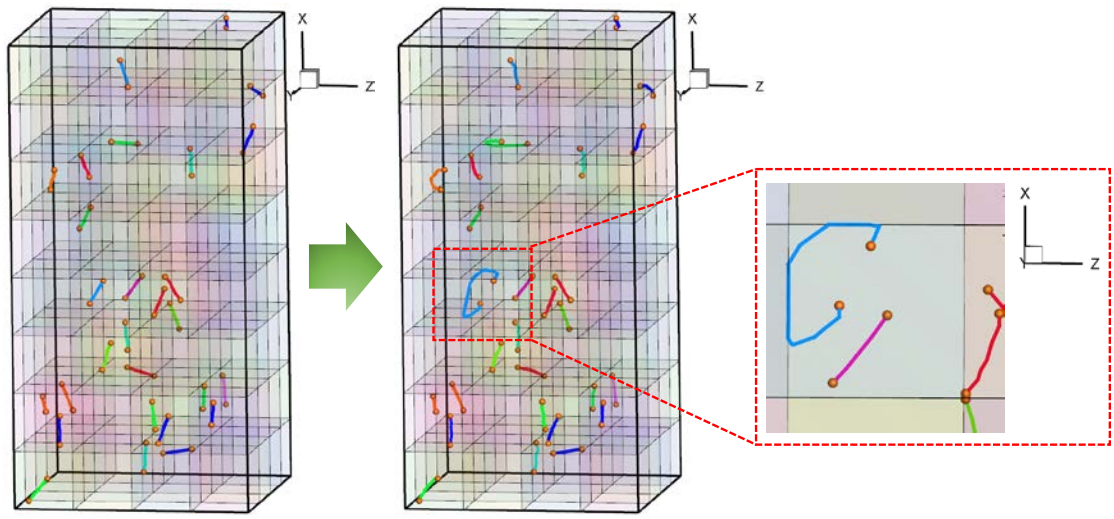

(a) (b)

Fig. 4. Dislocation confinement by GBs: dislocation structure of a sample with d=300b and d/l_{FR}=2. (a) Dislocation structure in the initial state, (b) the light blue dislocation line hits the GB surface and stops moving, as seen in the rectangular box and the corresponding enlarged figure on the right. The pinning points at two ends of a FR source are represented by the brown spheres in the figures.

To quantitatively analyze the impact of GB constraints on dislocation movement in polycrystalline metals, the data related to the activation and operation of FR sources are analyzed in more detail. Source operation can be characterized by the rotation of dislocation segments around their pinning points. As illustrated in Fig. 5a, the rotation angle of a segment between two sequential time steps can be determined as:

$$\Delta\theta = \left[\frac{\left(\boldsymbol{e}_i \times \boldsymbol{e}_i'\right)\cdot \boldsymbol{n}}{\left|\left(\boldsymbol{e}_i \times \boldsymbol{e}_i'\right)\cdot \boldsymbol{n}\right|}\right] \arccos\left(\boldsymbol{e}_i \cdot \boldsymbol{e}_i'\right) \tag{4}$$

where $\boldsymbol{e}_i$ and $\boldsymbol{e}_2'$ are the unit tangent vectors connecting the segment to its pinning point in two sequential time steps, and $\boldsymbol{n}$ is the slip plane normal vector. The square bracket in Eq. (4) corresponds to the sign of the incremental rotation angle: anti-clockwise rotations around $\boldsymbol{n}$ are counted as positive. The total rotation angle around a pinning point for n time steps can then be stated as

$$\sum \Delta\theta = \sum_{i=1}^{n} \left\{ \arccos\left(\boldsymbol{e}_i \cdot \boldsymbol{e}_i'\right) \cdot \left[\frac{\left(\boldsymbol{e}_i \times \boldsymbol{e}_i'\right) \cdot \boldsymbol{n}}{\left|\left(\boldsymbol{e}_i \times \boldsymbol{e}_i'\right) \cdot \boldsymbol{n}\right|} \right] \right\} \tag{5}$$

and the number of loops emitted from a FR source can be defined as

$$N = \frac{\left|\sum \Delta\theta_1\right| + \left|\sum \Delta\theta_2\right|}{4\pi} \tag{6}$$

where $\Delta\theta_1$ and $\Delta\theta_2$ are the rotation angles around both pinning points of a FR source, as shown in Fig. 5b. As illustrated in Figs. 5b-d, whether the source is activated or not can be determined by three configurations. The first one is that the initial FR source line bows out and becomes a semicircle (Fig. 5b). This configuration can also be simply defined as N=0.25 in Eq. (6). Before reaching the configuration in Fig. 5b, the dislocation may have been absorbed by GBs (Fig. 5c) or annihilated at free surfaces (Fig. 5d); such cases are also regarded as an indication of source activation. Sources meeting the criteria shown in Figs. 5b-d are in the following denoted as 'activated sources', and sources emitting more than one dislocation loop (N>1 in Eq. (6)) are denoted as 'operated sources'. The constraint of GBs on source operation can be quantified via the percentage of operated sources.

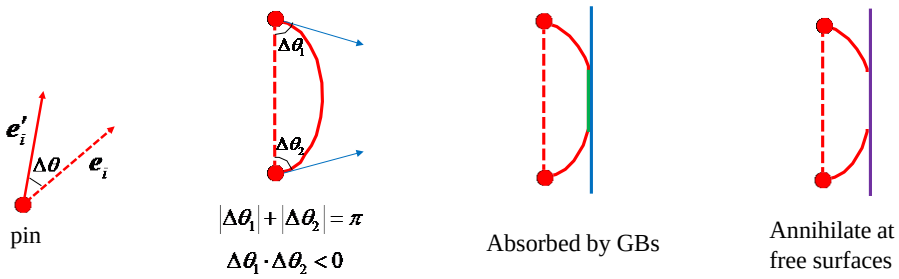

Fig. 5 Schematic illustration of dislocation rotation around a pinning point and criteria of source activation. (a) The dislocation segment rotates around the source pinning point by an angle $\Delta\theta$, (b-d) Criteria to determine the activation of a source: (b) the initially straight FR source line bows out and becomes a semicircle, (c) the dislocation is absorbed by GBs and (d) annihilated by free surfaces.

Fig. 6 presents quantitative results about the activation and operation of dislocation sources for the grain sizes of d=300b and d=400b. N_T is the total number of sources in the whole sample, N_A and N_O are the numbers of activated and operated sources, respectively. Figs. 6a and 6b give the percentages of activated sources N_A/N_T and operated sources N_O/N_A versus plastic strain ε_p before offset yielding (ε_p=0.1%) for different d/l_{FR} when d=300b. It is clearly seen that N_A/N_T increases with decreasing d/l_{FR} whereas the ratio of operated sources to activated sources tends to decrease as d/l_{FR} is reduced when ε_p>0.06%. This means that for small d/l_{FR}, although there is a higher probability of activating a source, the percentage of operated sources, which is an indication of the ability to operate the activated sources continuously, is reduced due to the confinement of dislocation movement by GBs. Corresponding data for d=400b are shown in Figs. 6d and 6e. As seen from these figures, the trends of the N_A/N_T and N_O/N_A curves are analogous to those for d=300b.

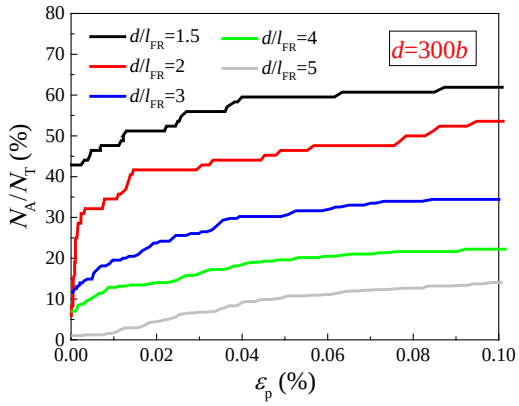

(a)

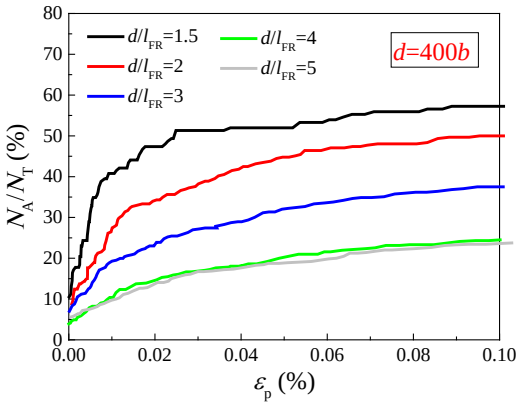

(d)

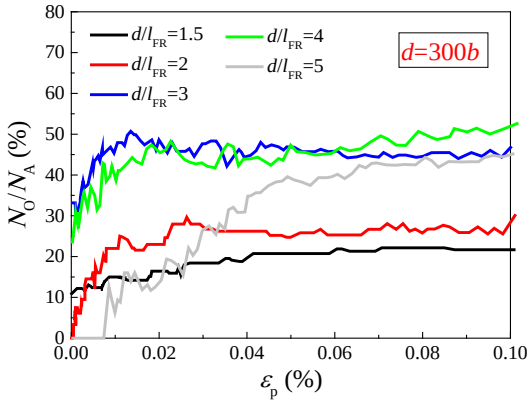

(b)

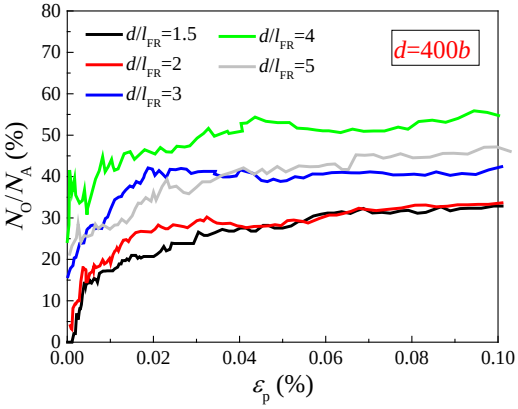

(e)

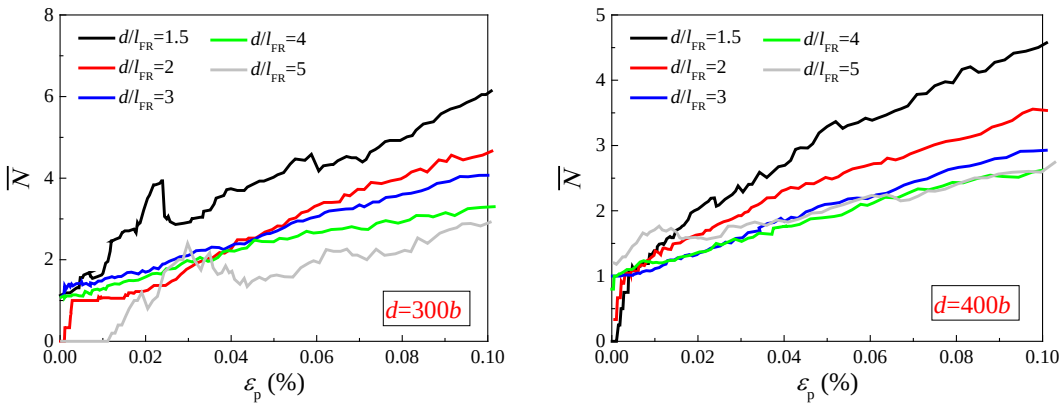

(c) (f)

Fig. 6. Results about the activation and operation of dislocation sources for grain sizes (a-c) d=300b and (d-f) d=400b. (a, d) Percentage of activated sources and (b, e) operated sources, (c, f) and an average number of emitted loops versus plastic strain for varied d/l_{FR}. N_T is the total number of sources in the whole sample, N_A and N_O are the numbers of activated and operated sources, respectively, and $\overline{N}$ is the average number of emitted loops per operated source.

The average number $\overline{N}$ of emitted loops, which is defined as $\overline{N} = \sum N/N_O$ (total number of loops divided by the number of operated sources), is plotted as a function of plastic strain in Figs. 6c (d=300b) and 6f (d=400b). We can observe from these figures that the average loop number $\overline{N}$ increases with decreasing d/l_{FR} for both d=300b and d=400b. This result can be understood as follows: Since there is a significant constraining effect on dislocation operation when d/l_{FR} is small, resulting in a low percentage of operated sources (see Figs. 6b and 6e), more loops must be emitted from each operated source to produce the plastic offset strain of 0.1%.

Fig. 7 gives, for the grain sizes of d=300b and d=400b, plots of $\overline{N}$, N_A/N_T and N_O/N_A versus d/l_{FR} at the plastic strain ε_p=0.1%. Interestingly, it is seen that N_A/N_T is nearly the same for both grain sizes. The decrease of N_A/N_T with increasing d/l_{FR} is related to the confining effect of GBs on dislocation operation. For small d/l_{FR}, the GBs impose strong constraints on dislocation movement. Hence, many sources need to be activated to accommodate the plastic strain, while the fraction of 'operated sources', N_O/N_A, is comparatively small, as shown in Fig. 7b.

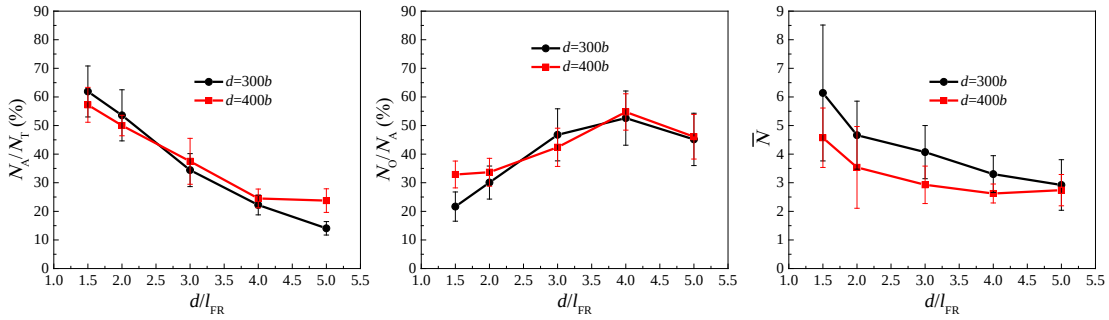

(a) (b) (c)

Fig. 7. (a) N_A/N_T (b) N_O/N_A and (c) $\overline{N}$ at the plastic strain of ε_p=0.1%, plotted versus d/l_{FR} for grain sizes d=300b and d=400b. $\overline{N}$ is the average number of emitted loops, N_T is the total number of sources in the whole sample, N_A and N_O are the numbers of activated and operated sources, respectively.

3.2 Effects of initial dislocation density and grain size on source activation

Section 3.1 has shown that source length and grain size have a significant influence on the activation and operation of sources. However, in real samples an entire spectrum of source lengths is present, and it is therefore important to investigate the behavior of samples containing a spectrum of source lengths. To this end, initial FR sources with random lengths ranging from $l_{FR}=d/5$ to $l_{FR}=d/1.5$ were randomly distributed in samples with different grain sizes (d=240b, d=300b, d=400b, d=500b, d=600b and d=700b). For each grain size, different initial dislocation densities (ρ_0=20 μm^{-2}, ρ_0=30 μm^{-2} and ρ_0=50 μm^{-2}), and thus different numbers of initial dislocation sources, have been simulated.

In Fig. 8, the three quantities N_A/N_T, N_O/N_A and $\overline{N}$ at the plastic strain of ε_p=0.1% are plotted versus grain size d for the three initial dislocation densities ρ_0=20 μm^{-2}, ρ_0=30 μm^{-2} and ρ_0=50 μm^{-2}. It shows that N_A/N_T and N_O/N_A are almost grain size independent and depend only weakly on initial dislocation density.

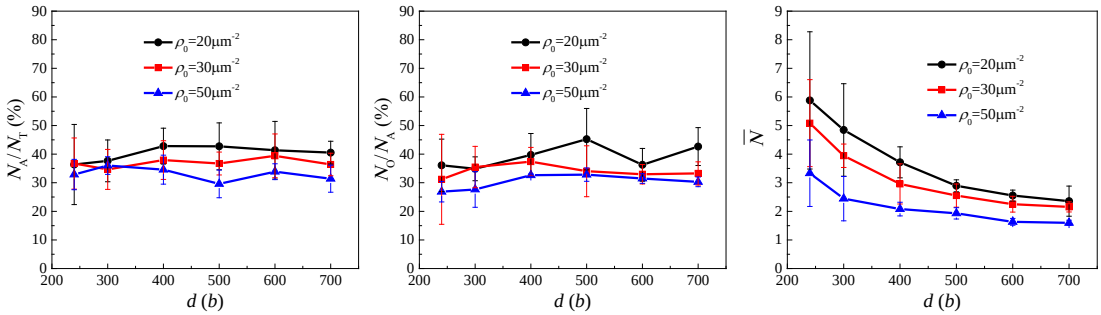

(a) (b) (c)

Fig. 8. (a) N_A/N_T (b) N_O/N_A and (c) $\bar{N}$ at the plastic strain of ε_p=0.1% versus grain size d for the initial dislocation densities of ρ_0=20 μm^{-2}, ρ_0=30 μm^{-2} and ρ_0=50 μm^{-2}. $\bar{N}$ is the average number of emitted loops per operated source, N_T is the total number of sources in the whole sample, N_A and N_O are the numbers of activated and operated sources, respectively.

As the overall number of operated sources per grain increases with increasing dislocation density, the average number $\bar{N}$ of emitted dislocations per operated source decreases with increasing dislocation density and increasing grain size. To understand this behavior, consider the strain created by loop emission from sources operated in one grain in the polycrystalline sample. The plastic strain ε_p equals

$$\varepsilon_p = \frac{1}{M}\frac{bS}{V} \tag{7}$$

where V is the volume of the grain and S is the total area swept by dislocations within this grain. The slipped area S_0 covered by one emitted loop is proportional to the cross-sectional area of the grain, i.e., $S_0=fd^2$ where f is a geometrical factor of the order of one. Combining with Eq. (7), the relation between plastic strain ε_p and average number $\bar{n}_O$ of loops per grain is expressed as

$$\varepsilon_p = \frac{b}{M}\frac{S}{V} = \frac{b}{M}\frac{\bar{n}_O S_0}{V} = \frac{b}{M}\frac{\bar{n}_O fd^2}{d^3} = \bar{n}_O \frac{f}{M}\frac{b}{d} \tag{8}$$

Eq. (8) shows that $\bar{n}_O$ linearly scales with the plastic strain ε_p for a specific grain size d. To verify this theoretical prediction, $\bar{n}_O \sim \varepsilon_p$ curves obtained from the simulations for all grain sizes are plotted in Figs. 9a (ρ_0=20 μm^{-2}), 9b (ρ_0=30 μm^{-2}) and 9c (ρ_0=50 μm^{-2}). As seen from Fig. 9, $\bar{n}_O$ scales almost linearly with the plastic strain for all grain sizes and all three initial dislocation densities. Moreover, the slope

of the curves is almost independent of initial dislocation density. This is consistent with the prediction in Eq. (8). $\bar{n}_0$ at ε_p=0.1% as a function of grain size d for three dislocation densities is displayed in Fig. 9d. Again, it shows that $\bar{n}_0$ roughly rises in proportion with grain size and does not depend on initial dislocation density, which is in good line with the scaling in Eq. (8).

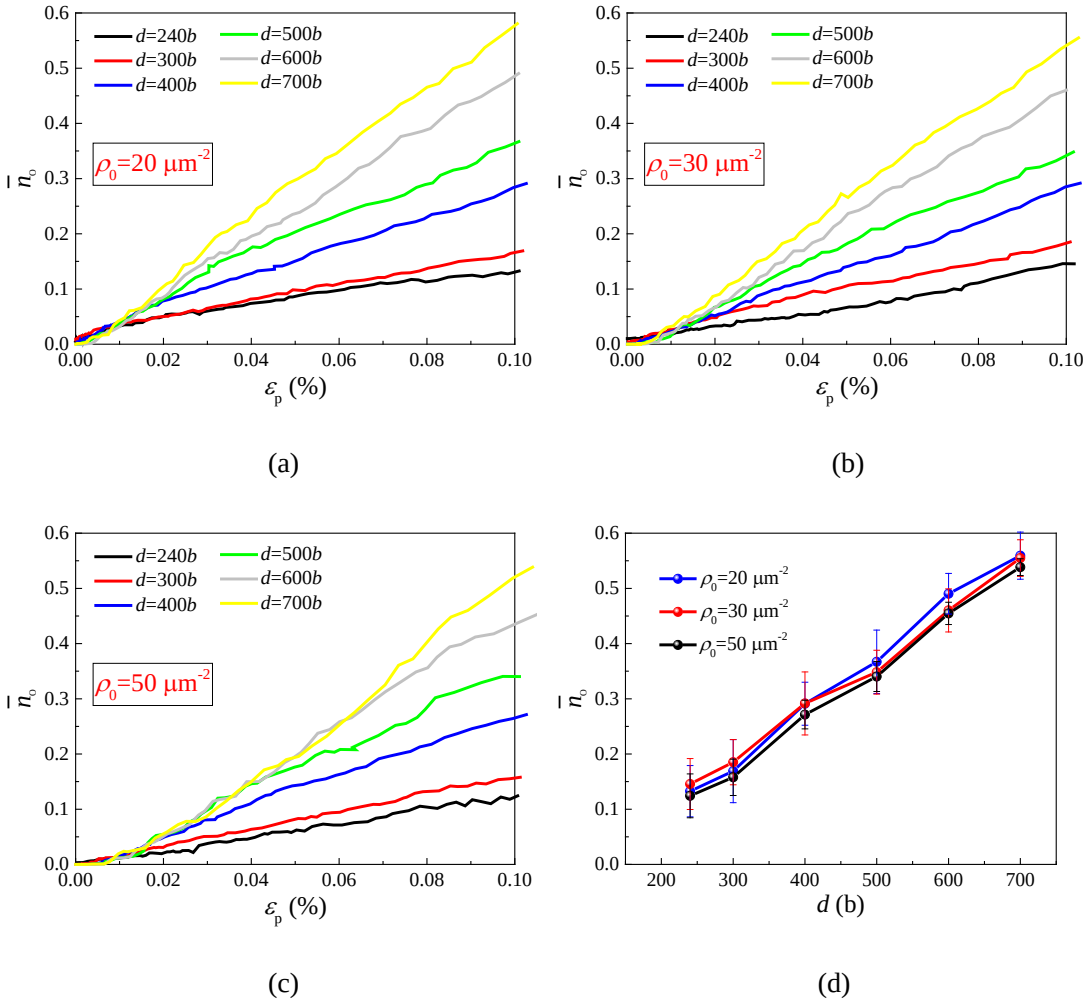

Fig. 9. Average loop number of each grain $\bar{n}_0$ (total number of emitted loops in the whole sample divided by the total grain number) versus plastic strain for the initial dislocation densities of (a) ρ_0=20 μm^{-2}, (b) ρ_0=30 μm^{-2} and (c) ρ_0=50 μm^{-2}, (d) $\bar{n}_0$ versus grain size d at 0.1% plastic strain.

4. Effects of grain size and initial dislocation density on yield stress

4.1 Simulation results

In order to investigate the effects of grain size and initial dislocation density on the yield stress of UFG polycrystals, simulation results of samples with six grain sizes:

d=240b, d=300b, d=400b, d=500b, d=600b and d=700b, and three initial dislocation densities: ρ_0=20 μm^{-2}, ρ_0=30 μm^{-2} and ρ_0=50 μm^{-2} were analyzed in detail. Again, the initial conditions in these simulations correspond to randomly distributed FR sources with a spectrum of source lengths ranging from $l_{FR}=d/5$ to $l_{FR}=d/1.5$. To examine the effect of GB penetrability on sample strength, the case with rigid GBs that act as impenetrable barriers to dislocation glide was also simulated for comparison.

The stress versus plastic strain curves before yielding for samples with various grain sizes and three different initial dislocation densities are shown in Fig. 10. The standard deviation bars at the plastic strains of 0.05% and 0.1% are presented for each curve in this figure. It can be seen that there is significant strain hardening for all cases, which also can be observed in the experiments in the literature (Gao et al., 2014; Li et al., 2021; Tsuji et al., 2002). Fig. 11a-d shows the corresponding strain hardening rate for all cases in Fig. 10. It can be found that the strain hardening rate decreases with increasing plastic strain, especially for the samples with penetrable grain boundaries (Fig. 11b-d). Besides, the figure shows that the strain hardening rate curves fluctuate intensively and there is no obvious trend for the relation between strain hardening rate and grain size. To examine the overall effect of grain size and initial dislocation density on the strain hardening rate, we averaged the strain hardening rate from ε_p=0 to ε_p=0.1%, as presented in Fig. 11e. It can be observed there is an overall trend that the strain hardening rate decreases as the grain size or the initial dislocation density increases. During the deformation stage from ε_p=0 to ε_p=0.1%, FR sources gradually activate and dislocations pile up in front of GBs, the overall stress-plastic strain response of a sample is a combined result of dislocation motions in the grain interior, back stresses caused by dislocation pile-ups in front of GBs, and the effect of slip transmission into neighboring grains which gradually reduces the hardening slope. Fig. 11e also shows that the strain hardening rate of the sample with rigid GB is larger than that of the penetrable GB counterpart. This is mainly due to the more significant dislocation pile-ups at GBs for the sample containing rigid GBs. To investigate the scatter of equivalent random realizations, the

standard deviations of stress at the plastic strains of ε_p=0.05% and ε_p=0.1% as a function of grain size are plotted in Fig. 11f for three initial dislocation densities. It can be seen that the standard deviation at ε_p=0.1% is larger than that of ε_p=0.05% and that the standard deviation decreases as the initial dislocation density increases. No systematic grain size dependency can be discerned. These observations indicate that the scatter of flow stresses is because the samples with higher initial dislocation density have more dislocation sources and thus decrease the scatter of realizations. In addition, at ε_p=0.05%, the standard deviation for the rigid GB case is similar to that of penetrable GB one, but has a lower value at ε_p=0.1%. This is because the dislocation density for the rigid GB sample is greatly larger than that of penetrable sample when the plastic strain reaches up to 0.1%.

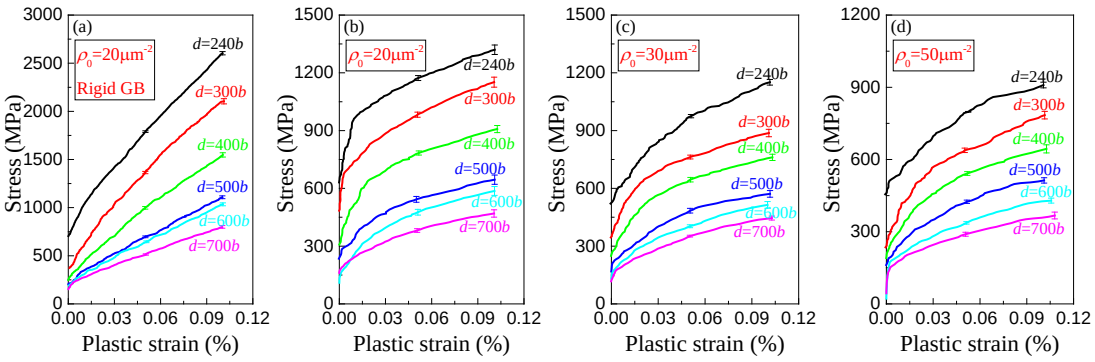

Fig. 10. (a) Stress versus plastic strain at various grain sizes for samples containing rigid GBs, with initial dislocation density ρ_0=20 μm^{-2}. (b-d) Results for samples containing penetrable GBs, with three different initial dislocation densities: (b) ρ_0=20 μm^{-2}, (c) ρ_0=30 μm^{-2}, (d) ρ_0=50 μm^{-2}.

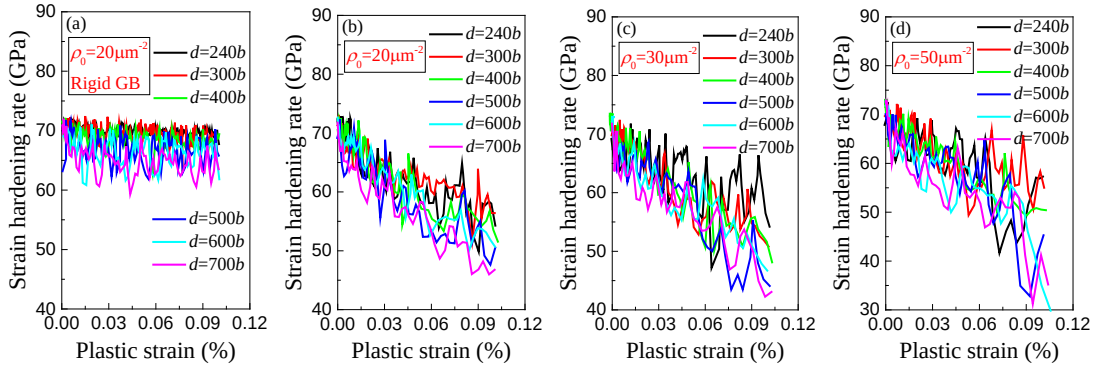

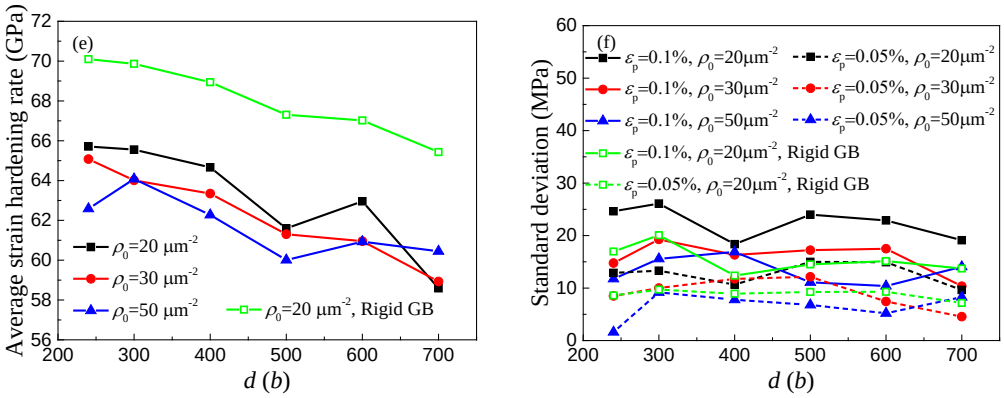

Fig. 11. (a) Strain hardening rate versus plastic strain at various grain sizes for samples containing rigid GBs, with initial dislocation density ρ_0=20 μm^{-2}. (b-d) Results for samples containing penetrable GBs, with three different initial dislocation densities: (b) ρ_0=20 μm^{-2}, (c) ρ_0=30 μm^{-2}, (d) ρ_0=50 μm^{-2}. (e) Average strain hardening rate (average over the data points from plastic strain ε_p=0 to ε_p=0.1%) versus grain size for four different samples. (f) Standard deviation of stress at the plastic strain levels of ε_p=0.05% and ε_p=0.1% versus grain size for four different samples.

The 0.1% offset yield stress versus grain size is presented in Fig. 12. It can be seen that the 0.1% offset yield stress of the samples decreases as the grain size increases, exhibiting a grain size effect, irrespective of GB penetrability and initial dislocation density. This typical size effect can be observed in experiments for a variety of polycrystalline metals (Dunstan and Bushby, 2014; Hall, 1951; Petch, 1953). Fig. 12 also shows that the strength of the sample with rigid GBs is much higher than that of samples with penetrable GBs.

Representative examples of dislocation structure evolution are presented in Fig. 13 for samples with rigid and penetrable GBs. In case of rigid GBs, with increasing plastic strain more and more dislocations accumulate along GBs, as shown in Figs. 13a-c. By contrast, when dislocation absorption at GBs and dislocation emission from GBs are allowed, the samples containing penetrable GBs exhibit less pronounced dislocation pile-ups, and at the offset yield strain substantial numbers of emitted dislocations (colored in green in Fig. 13f) can be observed in the material. From Fig. 12, it can also be seen that, both for samples with penetrable and samples with impenetrable GBs, the flow stress for a given grain size d decreases as the initial

dislocation density increases. This effect can be explained by the fact that, in the range of grain sizes and initial dislocation densities investigated here, the yield stress is mainly dominated by source activation (El-Awady, 2015). Dislocation-dislocation interactions give rise to a Taylor-type strength contribution which is proportional to the square root of dislocation density but, for the parameters considered here, this Taylor stress is quite weak compared to the stress required to activate a FR source, as will be discussed in detail in Section 4.3. For samples with higher initial dislocation density, and therefore a higher number of FR sources, there is a higher probability of finding weak sources that can be activated at low stress. Moreover, the total number of sources is larger, which means that each source needs to emit a smaller number of loops to accommodate the offset plastic strain. As a consequence, dislocation pile-ups and the concomitant back stresses are reduced. As a result, the yield stress decreases with increasing dislocation density, as shown in Fig. 12. (Balint et al., 2008) conducted 2D DDD simulations of tensile deformation of polycrystals and also found that the yield stress of samples with low dislocation source density is larger than that of samples with higher source densities. (Xu et al., 2019) used 2D DDD simulation to investigate indentation size effects and reported that the indentation pressures increase with decreasing initial source density. These studies demonstrate a regime of source limited dislocation plasticity which is quite similar to our simulation results.

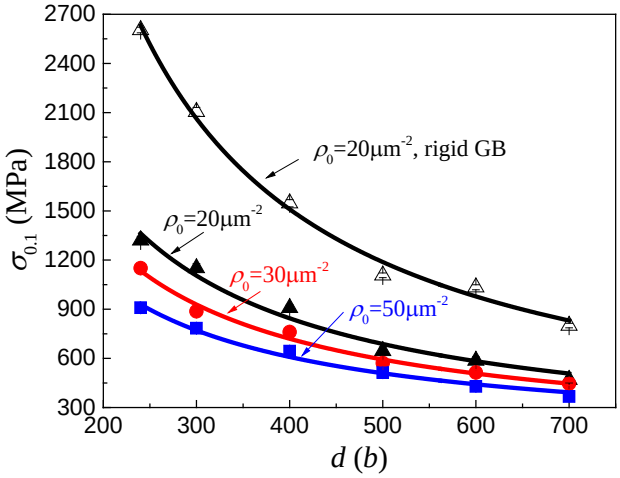

Fig. 12. The relation between 0.1% offset yield stress $\sigma_{0.1}$ and grain size d for samples with different initial dislocation densities: ρ_0=20 μm^{-2}, ρ_0=30 μm^{-2} and ρ_0=50 μm^{-2}. The data points

represent the simulated results while the solid curves are fitted by Eq. (9). For ρ_0=20 μm^{-2}, results for samples with rigid GBs are also plotted.

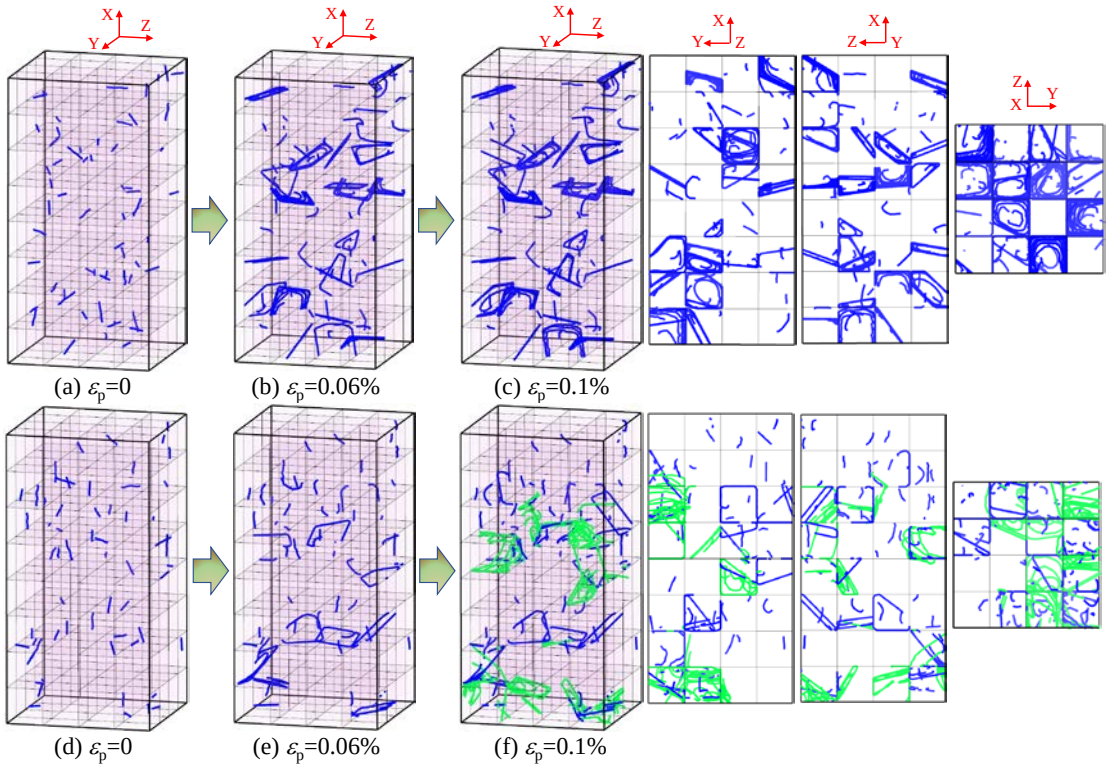

Fig. 13. Representative dislocation arrangements at plastic strains of ε_p=0, 0.06% and 0.1% for polycrystalline samples with (a-c) rigid GBs and (d-f) penetrable GBs. The three figures on the right side of (c) and (f) show the corresponding dislocation structure in different projections. The emitted dislocation lines are colored in green, whereas dislocations coming from sources in the grain interior are marked as blue lines. Grain size 400*b*, initial dislocation density 20 μm^{-2}.

4.2 Hall–Petch-like relationship

The relationship between grain size d and yield stress σ_y for polycrystalline metals can be described by a Hall–Petch-like formula as follows:

$$\sigma_y = \sigma_0 + kd^{-n} \tag{9}$$

where σ_0 is the yield stress of the single crystal or can be thought of as the yield stress of a very coarse-grained, untextured polycrystal. k and n are fitting parameters. The value of n usually ranges from 0.5 to 1 depending on many aspects like grain size range and initial dislocation density. When n=0.5, Eq. (9) reduces to the well-known Hall–Petch relation. Fits of Eq. (9) to the numerical results are presented in Fig. 12.

Note that the values of σ_0 are set to $\sigma_0 = M\alpha Gb\sqrt{\rho_0}$, representing Taylor hardening due to dislocation interactions in the coarse-grained, untextured polycrystal. Such an expression for σ_0 implies that σ_0 is assumed to be dependent on initial dislocation density but independent on grain size. The exponents *n* obtained from the simulations for different cases are summarized in Table 1. It can be seen from Table 1 that the values of *n* range from 0.91 to 0.98 for the cases with penetrable GBs, which is different from *n*=0.5 in the classical Hall–Petch relation. The experimental data presented in (Ohno and Okumura, 2007) show that the exponent *n* increases from approximately 0.5 to 1.0 for grain sizes less than about 5 μm, which is consistent with present simulation results. Besides, Table 1 shows that the value of *n* for the sample with rigid GBs is around 14% larger than that with penetrable GBs, indicating an overestimated grain size dependence when the GB is assumed to be an impenetrable barrier for dislocation motion. This result is consistent with a previous two-dimensional DDD study (Huang et al., 2020). Furthermore, as shown in Table 1, the value of *n* tends to decrease as the initial dislocation density increases. This trend is in good agreement with the results of former crystal-plasticity-based finite element simulations (Ohashi et al., 2007) and two/three-dimensional DDD simulations (Balint et al., 2008; El-Awady, 2015) in the literature.

Table 1 Values of exponent *n* in Eq. (9) obtained from simulations.

Cases	ρ_0=20 μm^{-2} (rigid GB)	ρ_0=20 μm^{-2}	ρ_0=30 μm^{-2}	ρ_0=50 μm^{-2}
Exponent *n*	1.113	0.978	0.947	0.913

4.3 Dislocation density increase and Taylor hardening

The evolution of total dislocation density versus plastic strain is plotted in Figs. 14a and 14b for ε_p<0.1% and three different initial dislocation densities. It is seen that the dislocation density increases with plastic strain in all cases. The existence of GBs in polycrystalline metals affects this increase in two distinct manners: First, the constraining effect of GBs delimits the dislocation mean free path, leading to enhanced dislocation storage in grains with operating sources. Second, dislocation emission from GBs may transfer slip into grains where no favorable source

configurations are present, leading to a further increase of dislocation density with plastic strain. This can be witnessed in the representative dislocation structure evolution shown in Figs. 13e and 13f, where dislocation pile-up in the vicinity of GBs and dislocation emission from GBs can both be clearly observed. Figs. 14a and 14b demonstrate that the dislocation density increases more strongly in samples with smaller grain size, irrespective of initial dislocation density. This grain-size dependence of dislocation density evolution is qualitatively in line with experimental results (Hansen, 1977; Hommel and Kraft, 2001). For the sake of clarity, the dislocation density increase at the plastic strain of 0.1%, ($\rho_{0.1}-\rho_0$), is shown in Fig. 14c as a function of grain size d. Following our discussion of loop accumulation in Section 3.2, the evolution and the grain-size dependence of dislocation density can be analyzed as follows: One loop emitted from an operated source and stopped at the GB has a line length of $l=4f'd$ where f' is a geometrical factor of the order of one. The dislocation density (line length per unit volume) is then obtained from the mean number $\bar{n}_{\mathrm{O}}$ of loops per grain as

$$\rho = \bar{n}_{\mathrm{O}} \frac{l}{V} = 4 f' \frac{\bar{n}_{\mathrm{O}}}{d^2} \tag{10}$$

Combining Eq. (8) and Eq. (10), we can obtain the rate of dislocation density increase per unit plastic strain as

$$\frac{\mathrm{d}\rho}{\mathrm{d}\varepsilon_{\mathrm{p}}} = \frac{4Mf'}{f} \cdot \frac{1}{bd} \tag{11}$$

Eq. (11) means that the dislocation density ρ scales linearly with plastic strain ε_{p} for given grain size, this is in line with the overall trend of simulation results shown in Fig. 14. Thus the dislocation density increase can be expressed as follows

$$\rho - \rho_0 = \frac{4Mf'}{fbd} \varepsilon_{\mathrm{p}} \tag{12}$$

where ρ_0 is the initial dislocation density, which is equal to the dislocation density at $\varepsilon_{\mathrm{p}}=0$. Eq. (12) indicates that $\rho-\rho_0$ should be proportional to ε_{p} and independent on the initial dislocation density. This agrees well with the behavior of Figs. 14a and 14b: for all grain sizes, the three curves with initial dislocation densities of ρ_0=20 μm^{-2},

ρ_0=30 μm^{-2} and ρ_0=50 μm^{-2} almost coincide. Fig. 14c shows the variation of $\rho_{0.1}-\rho_0$ as a function of grain size d for samples with three different initial dislocation densities. It can be observed that again all three curves almost coincide. An inverse proportionality with grain size d as predicted by Eq. (12) is observed for grain sizes from 400b onwards. For smaller grain sizes, Eq. (12) overestimates dislocation density accumulation. This is easy to understand: The assumption underlying Eq. (12), namely that the entire dislocation line length of an emitted loop is deposited at the GB, provides an upper estimate for the stored dislocation length. In samples where absorption/emission processes take place, this length must be corrected for the absorbed segments. This correction is pronounced in samples with small grain size, where the high overall stress level facilitates absorption at GBs, while at the same time the absorbed segments make up a relevant fraction of the overall loop length. Conversely, for grains above d=400b we may conclude that dislocation storage is mainly controlled by their pile up at GBs, whereas dislocation density reduction by absorption at GBs leads only to a minor correction.

According to Taylor's hardening theory, the shear stress resulting from mutual dislocation interactions is proportional to the square root of dislocation density, i.e.,

$$\tau_{\mathrm{f}} = \alpha G b \sqrt{\rho} \tag{13}$$

where α is a constant and G is the shear modulus of the sample, respectively. The tensile yield stress due to Taylor hardening can be correlated with the shear stress in Eq. (13) by

$$\sigma_{\mathrm{f}} = M \tau_{\mathrm{f}} \tag{14}$$

Fig. 15 displays the comparison of yield stress from simulations and obtained by Eqs. (13) and (14). It should be emphasized that the dislocation densities in Eq. (13) are the values at ε_{p}=0.1%. It can be clearly observed from Fig. 15 that the yield stresses evaluated from Eq. (13) are significantly lower than the simulated ones, especially for samples with small grain sizes. This suggests that, in the range of grain sizes and dislocation densities investigated here, the yield stress of polycrystalline metals is

dominated by grain size effects, whereas direct dislocation-dislocation interactions are of secondary importance.

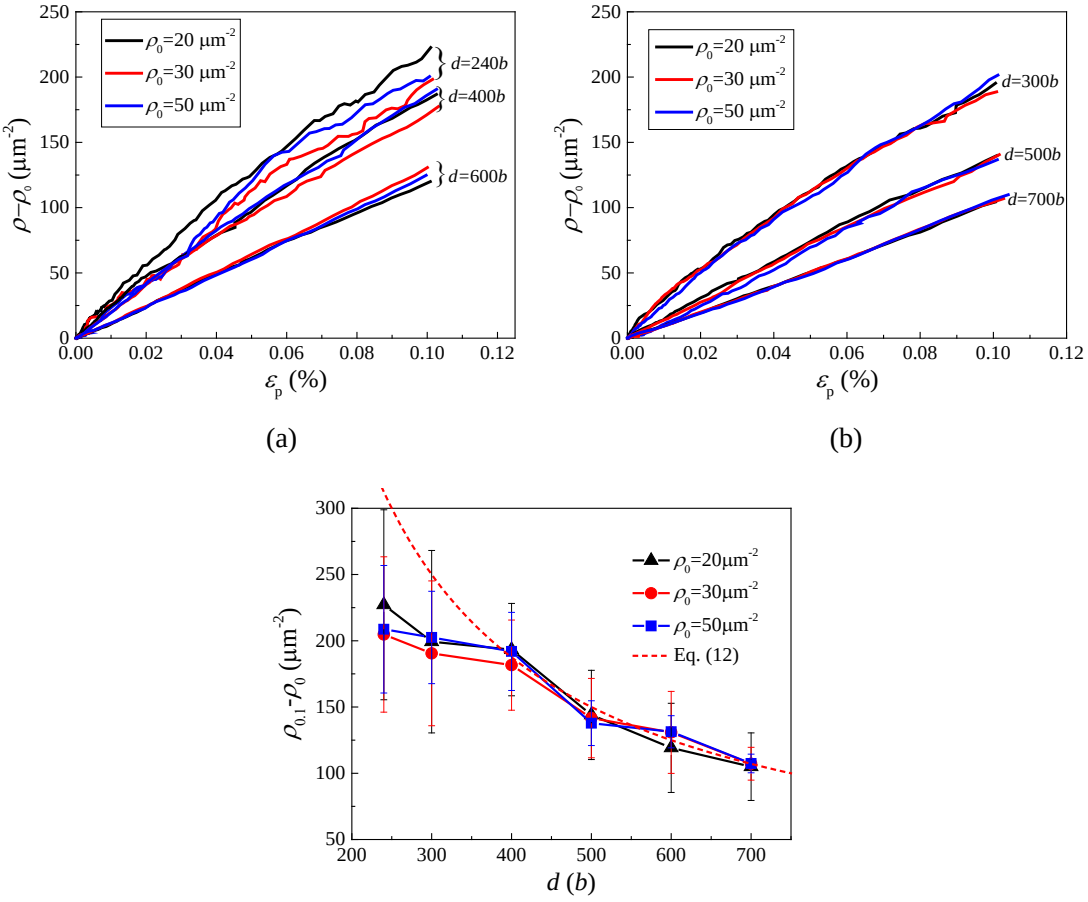

Fig. 14. (a, b) Dislocation density increment, $\rho-\rho_0$, versus plastic strain, ε_p, for polycrystalline samples with different initial dislocation densities and grain sizes, (c) dislocation density increment at ε_p=0.1%, $\rho_{0.1}-\rho_0$, versus grain size, d, for three different initial dislocation densities, a fit of Eq. (12) with (Mf'/f) = 1.03 is also shown in the figure.

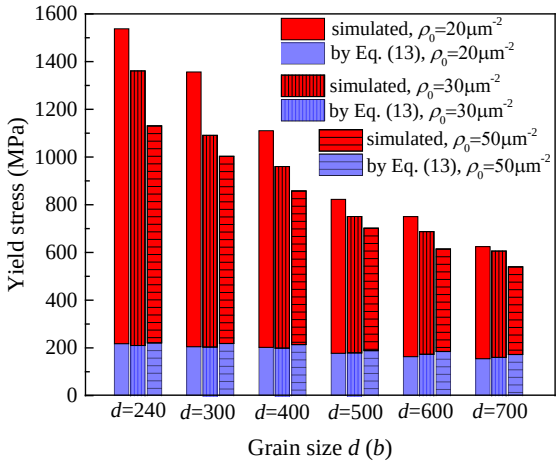

Fig. 15. Yield stresses obtained from simulations and Eq. (13) for varied grain sizes and three different initial dislocation densities.

4.4 Unified yield stress model

Our investigation in Section 4.1, 4.2 and 4.3 has demonstrated that, for the grain sizes and dislocation densities investigated here, grain size effects arise mainly from the constraining effect of dislocations on the operation of sources in the grain interior. To quantify this effect, we refer to the results from El-Awady (El-Awady, 2015), who carried out a large number of DDD simulations and then proposed a unified model that considered the combined effect of initial dislocation density and an extrinsic length scale D (grain size or micropillar diameter). In his model, the yield stress σ_y of samples with extrinsic length scale D is expressed as

$$\tau_y = \frac{\beta G}{D\sqrt{\rho_0}} + \alpha G b \sqrt{\rho_0} \tag{15}$$

$$\sigma_y = M \tau_y \tag{16}$$

where ρ_0 is the initial dislocation density of the sample and β is a fitting parameter. The first term on the right-hand side of Eq. (15) was interpreted as the strength of the weakest dislocation sources. In our simulations of samples containing a spectrum of source lengths, these correspond to sources with length close to $d/4$ that are located close to the grain center. The second term in Eq. (15), which is similar to Eq. (13), accounts for Taylor hardening.

To adapt the model of El-Awady to the present situations, we identify the length scale D with the grain size d. Furthermore, we note that the source density, which governs the strength of the weakest sources in the sense of extremal statistics, is controlled by the initial density ρ_0. Since the yield stress is taken from the flow stress at 0.1% plastic strain, the dislocation density ρ_0 in the second term on the right side of Eq. (15) must be replaced by $\rho_{0.1}$ (dislocation density at ε_p=0.1%):

$$\tau_y = \frac{\beta G}{d\sqrt{\rho_0}} + \alpha G b\sqrt{\rho_{0.1}} \tag{17}$$

The global fit of Eqs. (17) and (16) to our simulation data for polycrystalline metals with different grain sizes and initial dislocation densities is presented in Fig. 16a. Note that the forest hardening coefficient α is chosen as 0.57, as used in El-Awady's model (El-Awady, 2015). A common fit parameter β is used for all three curves. The fitted value of the parameter is 1.13×10^{-2}. It can be seen from Fig. 16a that the model in Eq. (17) can well describe the trend of the simulation data.

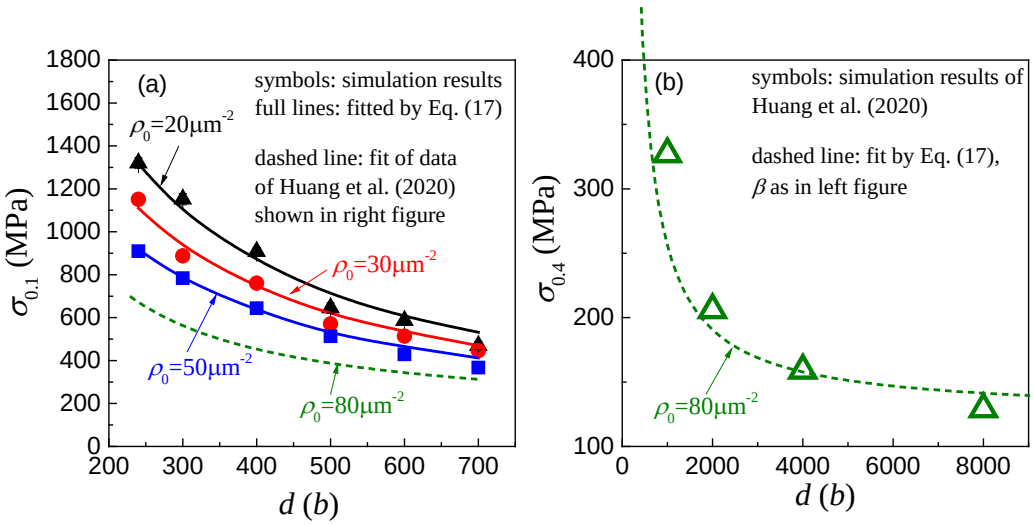

Fig. 16. (a) 0.1% offset yield strength $\sigma_{0.1}$ versus grain size d for different initial dislocation densities ρ_0: simulation results and fit by Eq. (17); (b) offset yield strength $\sigma_{0.4}$, simulation results of (Huang et al., 2020) and fit by Eq. (17). The dashed lines in (a) and (b) represent the same fit to the data of (Huang et al., 2020).

To demonstrate the range of applicability of Eq. (17), we used the same equation to model the data of (Huang et al., 2020) who used a 2D DDD-XFEM (extended finite element method) coupling framework to investigate the effect of grain size on the yield stress of polycrystalline aluminum. As in the present study, the grain boundaries were also assumed to be penetrable to dislocations in their framework. The initial (dislocation) source density was $\rho_0 = 80\ \mu m^{-2}$. Despite the significant differences in the simulation method and the fact that a larger offset strain of 0.4% was used by Huang et al., their grain size dependence is well represented by our fits of Eq. (17) without any need to adjust the parameter β, which can be directly transferred from our fits. This agreement, as demonstrated in Fig. 16b, confirms that our relationship can be used to represent data which pertain to grain sizes and dislocation densities well above those considered in our own simulations (note the different x axis range in Fig. 16a and b).

Eq. (17) is valid for samples containing a sufficiently wide spectrum of source lengths, such that yielding is controlled by 'optimal' sources of length $\approx d/4$. If we prescribe a fixed source length, on the other hand, the model in Eq. (17) needs to be extended to capture the effect of the additional length scale introduced by the source length. Such an effect is, according to our results of Section 3.1, expected when $d/l_{FR}<4$. For this case, we express the source-length dependent yield stress in generalization of Eq. (17) as

$$\begin{aligned} &\tau_y = \frac{\beta G}{d\sqrt{\rho_0}}\Phi^*\left(\frac{d}{l_{FR}}\right) + \alpha G b\sqrt{\rho_{0.1}} \\ &\Phi^*(x) = x\Phi(x), \quad \Phi(4) = 1 \\ &\sigma_y = M\tau_y \end{aligned} \tag{18}$$

where Φ or Φ^* can be regarded as source-grain hardening interaction functions, their functional form is chosen as:

$$\begin{cases} \Phi(x) = \left(\dfrac{x}{4}\right)^q & \text{(when } x < 4\text{)} \\ \Phi(x) = \left(\dfrac{8}{x^2} + \dfrac{1}{2}\right)^{1/2} & \text{(when } x > 4\text{)} \end{cases} \tag{19}$$

where q is a fitting parameter. The functional form chosen above has the following rationale. In the work of (Friedman and Chrzan, 1998), the superposition of Hall-Petch hardening and source hardening was analyzed within the framework of the classical HP theory based on dislocation pile-up at penetrable GBs. They found that in this case the source activation stress τ_s and the Hall-Petch contribution τ_{HP} to the flow stress superimpose according to $\tau_y = \sqrt{\tau_{HP}^2 + \tau_s^2}$. This relation was derived under the assumption that the source extension is small as compared to the pile-up length/grain size, which is similar to cases of $d/l_{FR} > 4$ in our simulations. So the above-proposed form in Eq. (19) combines two expressions for two distinct regimes:

(1) At $d/l_{FR} < 4$, we have a mutual confinement regime. On the one hand, the grain boundary confines the source. On the other hand, the source extension reduces the space for pile-up formation. Hence, the effective grain size both effects mutually exacerbate each other to produce an enhanced strengthening effect.

(2) At $d/l_{FR} > 4$, we have an additive hardening regime. Here the effects of pile-up formation at GBs and the stress needed to operate the source mutually add up, in a root-mean-square manner as expected from pile-up theory, as discussed above.

The fit values obtained from Eq. (18) for different grain sizes with varied d/l_{FR} are plotted together with the simulation results in Fig. 17. The fitted value of the parameter q in Eq. (19) is −1.5. It is noteworthy that the coefficients α and M in for this fit are identical to those in Fig. 16. As seen in Fig. 17, the fitted results can well capture the trend of the simulation data.

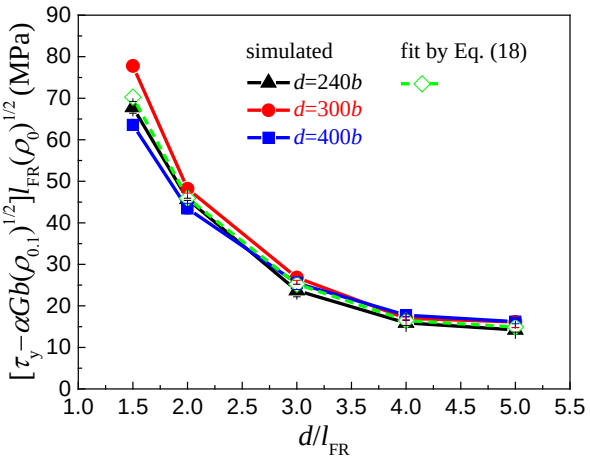

Fig. 17. Source-size dependence of yield stress: simulated results and fit by Eq. (18).

It should be mentioned that compared with the HP-like relation in Eq. (9), the model in Eq. (17) can simultaneously incorporate both the effects of grain size and initial dislocation density by only one fit parameter – a result which can be transferred to continuum constitutive models in order to describe the grain size dependence of the yield stress. Moreover, Eq. (17) can also be extended to account for the source length effect, as stated in Eq. (18). Note that our results go well beyond previous approaches to describe the superposition of different hardening mechanisms: as expressed by Eqs. (18), (19) the coupled effects of source length, grain size and initial dislocation density are non additive and non monotonic, giving rise to complex and non trivial dependency of the flow stress on key microstructure parameters.

5. Conclusions

In the current study, a polycrystal model containing multiple cube-shaped grains with randomly distributed orientations has been constructed in a three-dimensional DDD framework. The grain boundaries implemented in this model consider the mechanisms of dislocation absorption at GBs and dislocation emission from GBs. The constructed polycrystal model is then used to investigate the effects of source length and grain size on the yield stress of polycrystalline metals. The influences of dislocation activation and source operation on the size effects are analyzed in detail. The main conclusions can be summarized as follows:

(1) The yield stress of polycrystalline metals is closely related to the ratio of grain size to FR source length. The polycrystalline sample has the lowest yield stress when the FR source length is around $d/4$. Due to GB confinement of dislocation motion, the simulated yield stress is significantly higher than the critical stress required to activate a bulk source if the source size is larger than $d/4$.

(2) The simulation results show that the yield stress of polycrystalline samples with impenetrable GBs is more than twice as high as that with penetrable GBs owing to the severe dislocation pile-ups in front of GBs. This suggests that the assumption of impenetrable GB in DDD simulations of the deformation of polycrystalline metals, for some cases, may overestimate grain size effects.

(3) The simulations of the deformation of polycrystalline metals with different grain sizes show that the relationship between the yield stress and grain size of the samples does not obey the Hall–Petch law. The Hall–Petch exponent n for the cases studied here ranges from 0.91 to 0.98 depending on the initial dislocation density.

(4) The grain size dependence of the yield stress of polycrystalline metals is mainly controlled by dislocation activation. Taylor hardening coming from the mutual interactions of dislocations only contributes a minor fraction of the yield stress, especially when the grain size is relatively small.

(5) During the initial, grain boundary controlled deformation stage, the dislocation density increases linearly with plastic strain with a rate that does not depend on the initial dislocation density; a simple model was proposed to capture dislocation density evolution in this regime.

(6) A theoretical model is proposed that simultaneously accounts for the effects of source length, grain size, and initial dislocation density. This model matches the simulated data well and can be applied in continuum constitutive laws.

In conclusion, we comment on the range of validity of the present considerations. Our simulations pertain to situations where the grain size is comparable to typical dislocation source lengths and source spacings, such that $d\sqrt{\rho_0}$ is of the order of one.

In such situations, plastic flow in individual grains is controlled by single sources and their interaction with grain boundaries. For the present initial dislocation densities, this corresponds to behavior in the ultrafine- and nanograined regime. Size-dependent plasticity in coarse-grained structures requires a separate consideration which will be published elsewhere. Another point worth mentioning is that the dislocation spacings are comparable to the grain size in the present simulations. Thus, the systems we investigated here are very low-density systems. It is of interest to predict the situation in the denser systems based on our present simulation results. As shown in the conclusions mentioned above, the exponent n in the Hall-Petch-like relation decreases from 0.98 to 0.91 as the initial dislocation density increases from 20 to 50 μm^{-2}. Therefore, it is possible that the value of n reduces towards 0.5 (i.e. the conventional Hall-Petch relation) when the initial dislocation density is sufficiently high. In addition, the contribution of Taylor hardening for the yield strength will increase while the source effect will play a weaker role in the denser systems, as reflected by Eq. (17). We note that our choice of initial conditions (FR sources with strong pinning points) may somewhat over-estimate source efficiency and pile-up formation. There are alternative scenarios for deformation of UFG polycrystals: 1) Deformation in absence of efficient sources has been described by (Li et al., 2021), see also (Khan and Liu, 2016): If no sources are present in grain interiors, then intragranular dislocation motion readily gets exhausted. Deformation must then be sustained by emission of new dislocations from GBs, which in absence of supporting pile up stresses requires a significantly higher external stress level than in the present investigation. 2) If no dislocations are present in the grain interiors, deformation must from the onset proceed by dislocation emission from GBs – a process that may be assisted by dislocation debris deposited at GBs during prior processing e.g. by severe plastic deformation, and which requires even higher stress levels. Both situations 1) and 2) can be studied with the DDD-GB model used in the present work. To this end one just needs to change the initial conditions in the simulations. Instead of FR sources as initial conditions one needs to consider grain threading dislocations for case 1) and dislocations absorbed randomly at GBs for case 2). Investigation of these

situations is postponed to further study. Finally, for UFG materials, grain boundary mechanisms, such as grain boundary slip or rotation, may provide additional deformation pathways. A comprehensive DDD framework incorporating all these aspects is worth to establish in the future.

Acknowledgment

This work was supported by the National Natural Science Foundation of China (Grant Nos. 11672251 and 11872321) and Major Science and Technology Special Project of Sichuan Province (2020ZDZX0009). M. Zaiser also acknowledges support by DFG under grant 1Za 171 13-1 and the Chinese State Administration of Foreign Experts Affairs under Grant no. MS2016XNJT044.

References

Balint, D.S., Deshpande, V.S., Needleman, A., Van der Giessen, E., 2006. Discrete dislocation plasticity analysis of the wedge indentation of films. J. Mech. Phys. Solids 54, 2281-2303.

Balint, D.S., Deshpande, V.S., Needleman, A., Van der Giessen, E., 2008. Discrete dislocation plasticity analysis of the grain size dependence of the flow strength of polycrystals. Int. J. Plasticity 24, 2149-2172.

Bayerschen, E., Stricker, M., Wulfinghoff, S., Weygand, D., Böhlke, T., 2015. Equivalent plastic strain gradient plasticity with grain boundary hardening and comparison to discrete dislocation dynamics. Proceedings of the Royal Society A: Mathematical, Physical and Engineering Sciences 471, 20150388.

Bertin, N., Sills, R., Cai, W., 2020. Frontiers in the Simulation of Dislocations. Ann. Rev. Mater. Res. 50, 437-464.

Biner, S.B., Morris, J.R., 2002. A two-dimensional discrete dislocation simulation of the effect of grain size on strengthening behaviour. Model. Simul. Mater. Sc. 10, 617-635.

Biner, S.B., Morris, J.R., 2003. The effects of grain size and dislocation source density on the strengthening behaviour of polycrystals: a two-dimensional discrete dislocation simulation. Philosophical Magazine 83, 3677-3690.

Borg, U., 2007. A strain gradient crystal plasticity analysis of grain size effects in polycrystals. European Journal of Mechanics - A/Solids 26, 313-324.

Bulatov, V.V., Reed, B.W., Kumar, M., 2014. Grain boundary energy function for fcc metals. Acta Mater. 65, 161-175.

Chatterjee, S., Li, Y., Po, G., 2021. A discrete dislocation dynamics study of precipitate bypass mechanisms in nickel-based superalloys. Int. J. Plasticity 145, 103062.

Cordero, Z.C., Knight, B.E., Schuh, C.A., 2016. Six decades of the Hall–Petch effect – a survey of grain-size strengthening studies on pure metals. Int. Mater. Rev. 61, 495-512.

Cui, Y.N., Lin, P., Liu, Z.L., Zhuang, Z., 2014. Theoretical and numerical investigations of single arm dislocation source controlled plastic flow in FCC micropillars. Int. J. Plasticity 55, 279-292.

De Sansal, C., Devincre, B., Kubin, L.P., 2010. Grain Size Strengthening in Microcrystalline Copper: A Three-Dimensional Dislocation Dynamics Simulation. Key Engineering Materials 423, 25-32.

Dunstan, D.J., Bushby, A.J., 2013. The scaling exponent in the size effect of small scale plastic deformation. Int. J. Plasticity 40, 152-162.

Dunstan, D.J., Bushby, A.J., 2014. Grain size dependence of the strength of metals: The Hall–Petch effect does not scale as the inverse square root of grain size. Int. J. Plasticity 53, 56-65.

El-Awady, J.A., 2015. Unravelling the physics of size-dependent dislocation-mediated plasticity. Nature Communications 6, 5926.

Espinosa, H.D., Berbenni, S., Panico, M., Schwarz, K.W., 2005. An interpretation of size-scale plasticity in geometrically confined systems. Proceedings of the National Academy of Sciences of the United States of America 102, 16933-16938.

Espinosa, H.D., Panico, M., Berbenni, S., Schwarz, K.W., 2006. Discrete dislocation dynamics simulations to interpret plasticity size and surface effects in freestanding FCC thin films. Int. J. Plasticity 22, 2091-2117.

Evers, L.P., Brekelmans, W.A.M., Geers, M.G.D., 2004. Scale dependent crystal plasticity framework with dislocation density and grain boundary effects. Int. J. Solids Struct. 41, 5209-5230.

Fan, H., Aubry, S., Arsenlis, A., El-Awady, J.A., 2016. Grain size effects on dislocation and twinning mediated plasticity in magnesium. Scripta Mater. 112, 50-53.

Fan, H., Ngan, A.H.W., Gan, K., El-Awady, J.A., 2018. Origin of double-peak precipitation hardening in metallic alloys. Int. J. Plasticity 111, 152-167.

Fan, H., Wang, Q., El-Awady, J.A., Raabe, D., Zaiser, M., 2021. Strain rate dependency of dislocation plasticity. Nature Communications 12, 1845.

Friedman, L.H., Chrzan, D.C., 1998. Continuum analysis of dislocation pile-ups: Influence of sources. Philosophical Magazine A 77, 1185-1204.

Gao, S., Chen, M., Joshi, M., Shibata, A., Tsuji, N., 2014. Yielding behavior and its effect on uniform elongation in IF steel with various grain sizes. J. Mater. Sci. 49, 6536-6542.

Gray, G.T., Lowe, T.C., Cady, C.M., Valiev, R.Z., Aleksandrov, I.V., 1997. Influence of strain rate & temperature on the mechanical response of ultrafine-grained Cu, Ni, and Al-4Cu-0.5Zr. Nanostruct. Mater. 9, 477-480.

Guo, X., Sun, C., Wang, C., Jiang, J., Fu, M.W., 2021. Study of dislocation-twin boundary interaction mechanisms in plastic deformation of TWIP steel by discrete dislocation dynamics and dislocation density-based modeling. Int. J. Plasticity 145, 103076.

Guruprasad, P.J., Benzerga, A.A., 2008. Size effects under homogeneous deformation of single crystals: A discrete dislocation analysis. J. Mech. Phys. Solids 56, 132-156.

Hall, E.O., 1951. The deformation and ageing of mild steel: III Discussion of results. Proceedings of the Physical Society. Section B 64, 747-753.

Hansen, N., 1977. The effect of grain size and strain on the tensile flow stress of aluminium at room temperature. Acta Metallurgica 25, 863-869.

Hirth, J.P., Lothe, J., 1982. Theory of dislocations, Wiley, New York.

Hommel, M., Kraft, O., 2001. Deformation behavior of thin copper films on deformable substrates. Acta Mater. 49, 3935-3947.

Huang, M., Huang, S., Liang, S., Zhu, Y., Li, Z., 2020. An efficient 2D discrete dislocation Dynamics-XFEM coupling framework and its application to polycrystal plasticity. Int. J. Plasticity 127, 102647.

Huang, M., Li, Z., 2015. Coupled DDD–FEM modeling on the mechanical behavior of microlayered metallic multilayer film at elevated temperature. J. Mech. Phys. Solids 85, 74-97.

Huang, M., Liang, S., Li, Z., 2017. An extended 3D discrete-continuous model and its application on single- and bi-crystal micropillars. Model. Simul. Mater. Sc. 25, 035001.

Jamond, O., Gatti, R., Roos, A., Devincre, B., 2016. Consistent formulation for the Discrete-Continuous Model: Improving complex dislocation dynamics simulations. Int. J. Plasticity 80, 19-37.

Jiang, M., Devincre, B., Monnet, G., 2019. Effects of the grain size and shape on the flow stress: A dislocation dynamics study. Int. J. Plasticity 113, 111-124.

Jiang, M., Monnet, G., Devincre, B., 2021. On the origin of the Hall-Petch law: a 3D-Dislocation Dynamics simulation investigation. Acta Mater., 116783.

Keller, R.M., Baker, S.P., Arzt, E., 1998. Quantitative analysis of strengthening mechanisms in thin Cu films: Effects of film thickness, grain size, and passivation. J. Mater. Res. 13, 1307-1317.

Khan, A.S., Liu, J., 2016. A deformation mechanism based crystal plasticity model of ultrafine-grained/nanocrystalline FCC polycrystals. Int. J. Plasticity 86, 56-69.

Kumar, R., Székely, F., Van der Giessen, E., 2010. Modelling dislocation transmission across tilt grain boundaries in 2D. Comp. Mater. Sci. 49, 46-54.

Lefebvre, S., Devincre, B., Hoc, T., 2007. Yield stress strengthening in ultrafine-grained metals: A two-dimensional simulation of dislocation dynamics. J. Mech. Phys. Solids 55, 788-802.

Leung, P.S.S., Ngan, A.H.W., 2013. Size effect on the strength of micron-sized polycrystals – A dislocation dynamics simulation study. Scripta Mater. 69, 235-238.

Li, H., Gao, S., Tomota, Y., Ii, S., Tsuji, N., Ohmura, T., 2021. Mechanical response of dislocation interaction with grain boundary in ultrafine-grained interstitial-free steel. Acta Mater. 206, 116621.

Li, Z., Hou, C., Huang, M., Ouyang, C., 2009. Strengthening mechanism in micro-polycrystals with penetrable grain boundaries by discrete dislocation dynamics simulation and Hall–Petch effect. Comp. Mater. Sci. 46, 1124-1134.

Lu, S., Zhang, B., Li, X., Zhao, J., Zaiser, M., Fan, H., Zhang, X., 2019. Grain boundary effect on nanoindentation: A multiscale discrete dislocation dynamics model. J. Mech. Phys. Solids 126, 117-135.

Nicola, L., Van der Giessen, E., Needleman, A., 2005. Size effects in polycrystalline thin films analyzed by discrete dislocation plasticity. Thin Solid Films 479, 329-338.

Nicola, L., Xiang, Y., Vlassak, J.J., Van der Giessen, E., Needleman, A., 2006. Plastic deformation of freestanding thin films: Experiments and modeling. J. Mech. Phys. Solids 54, 2089-2110.

Ohashi, T., Kawamukai, M., Zbib, H., 2007. A multiscale approach for modeling scale-dependent yield stress in polycrystalline metals. Int. J. Plasticity 23, 897-914.

Ohno, N., Okumura, D., 2007. Higher-order stress and grain size effects due to self-energy of geometrically necessary dislocations. J. Mech. Phys. Solids 55, 1879-1898.

Petch, N.J., 1953. The cleavage strength of polycrystals. Journal of the Iron and Steel Institute 174, 25-28.

Quek, S.S., Chooi, Z.H., Wu, Z., Zhang, Y.W., Srolovitz, D.J., 2016. The inverse hall–petch relation in nanocrystalline metals: A discrete dislocation dynamics analysis. J. Mech. Phys. Solids 88, 252-266.

Shishvan, S.S., Van der Giessen, E., 2010. Distribution of dislocation source length and the size dependent yield strength in freestanding thin films. J. Mech. Phys. Solids 58, 678-695.

Srivastava, K., El-Awady, J.A., 2017. Deformation of magnesium during c-axis compression at low temperatures. Acta Mater. 133, 282-292.

Tsuji, N., Ito, Y., Saito, Y., Minamino, Y., 2002. Strength and ductility of ultrafine grained aluminum and iron produced by ARB and annealing. Scripta Mater. 47, 893-899.

Vattré, A., Devincre, B., Feyel, F., Gatti, R., Groh, S., Jamond, O., Roos, A., 2014. Modelling crystal plasticity by 3D dislocation dynamics and the finite element method: The Discrete-Continuous Model revisited. J. Mech. Phys. Solids 63, 491-505.

Venkatraman, R., Bravman, J.C., 1992. Separation of film thickness and grain boundary strengthening effects in Al thin films on Si. J. Mater. Res. 7, 2040-2048.

von Blanckenhagen, B., Arzt, E., Gumbsch, P., 2004. Discrete dislocation simulation of plastic deformation in metal thin films. Acta Mater. 52, 773-784.

von Blanckenhagen, B., Gumbsch, P., Arzt, E., 2001a. Discrete dislocation simulation of thin film plasticity. MRS Proceedings 673, P2.3.

von Blanckenhagen, B., Gumbsch, P., Arzt, E., 2001b. Dislocation sources in discrete dislocation simulations of thin-film plasticity and the Hall-Petch relation. Model. Simul. Mater. Sc. 9, 157-169.

von Blanckenhagen, B., Gumbsch, P., Arzt, E., 2003. Dislocation sources and the flow stress of polycrystalline thin metal films. Phil. Mag. Lett. 83, 1-8.

Xu, Y., Balint, D., Dini, D., 2019. A new hardness formula incorporating the effect of source density on indentation response: A discrete dislocation plasticity analysis. Surface and Coatings Technology 374, 763-773.

Xu, Y., Ruebeling, F., Balint, D., Greiner, C., Dini, D., 2021. On the origin of microstructural discontinuities in sliding contacts: A discrete dislocation plasticity analysis. Int. J. Plasticity 138, 102942.

Yellakara, R.N., Wang, Z., 2014. A three-dimensional dislocation dynamics study of the effects of grain size and shape on strengthening behavior of fcc Cu. Comp. Mater. Sci. 87, 253-259.

Yu, D., Spaepen, F., 2004. The yield strength of thin copper films on Kapton. J. Appl. Phys. 95, 2991-2997.

Záležák, T., Svoboda, J., Dlouhý, A., 2017. High temperature dislocation processes in precipitation hardened crystals investigated by a 3D discrete dislocation dynamics. Int. J. Plasticity 97, 1-23.

Zbib, H.M., Diaz de la Rubia, T., 2002. A multiscale model of plasticity. Int. J. Plasticity 18, 1133-1163.

Zbib, H.M., Rhee, M., Hirth, J.P., 1998. On plastic deformation and the dynamics of 3D dislocations. Int. J. Mech. Sci. 40, 113-127.

Zhang, X., Aifantis, K.E., Senger, J., Weygand, D., Zaiser, M., 2014. Internal length scale and grain boundary yield strength in gradient models of polycrystal plasticity: How do they relate to the dislocation microstructure? J. Mater. Res. 29, 2116-2128.

Zhang, X., Lu, S., Zhang, B., Tian, X., Kan, Q., Kang, G., 2021. Dislocation–grain boundary interaction-based discrete dislocation dynamics modeling and its application to bicrystals with different misorientations. Acta Mater. 202, 88-98.

Zhou, C., LeSar, R., 2012. Dislocation dynamics simulations of plasticity in polycrystalline thin films. Int. J. Plasticity 30-31, 185-201.